



Destabilization of buried carbon under changing moisture regimes

Teneille Nel*¹, Manisha Dolui*¹, Abbygail R. McMurtry², Stephanie Chacon¹, Joseph A. Mason³, Laura M. Phillips², Erika Marin-Spiotta³, Marie-Anne de Graaff², Asmeret Asefaw Berhe¹, and Teamrat A. Ghezzehei¹

Correspondence: Teneille Nel* (tnel@ucmerced.edu)

*These authors contributed equally to this work.

Abstract.

Paleosols formed by the burial of topsoil during landscape evolution can sequester substantial amounts of soil organic carbon (SOC) over millennia due to protection from surface disturbances. We investigated the moisture sensitivity of buried SOC storage in the Brady paleosol, a loess-derived soil in Nebraska, USA, where historical aeolian deposition during the Pleistocene–Holocene transition buried soils up to 6 m deep. Topsoils from erosional (up to 1.8 m depth) and depositional (up to 5.8 m depth) transects were incubated under two moisture regimes - continuous wetting (60% water-holding capacity) and repeated drying–rewetting - to assess SOM vulnerability to changing hydrologic conditions.

SOC decomposition rates modeled from CO_2 fluxes were consistently higher in erosional than depositional settings, with surface re-exposure of Brady soils enhancing microbial accessibility and destabilization. A two-pool model showed that >96% of SOC was stored in a slow-cycling pool, particularly in deeply buried soils where stabilization was linked to mineral association, fine particles, and Ca-mediated flocculation. However, this pool decomposed more rapidly in shallower Brady soils (higher turnover rate relative to buried soil), reflecting increased microbial responsiveness to surface-driven processes.

Drying–rewetting cycles caused greater SOC losses from Brady soils than continuous wetting, despite the dominance of the slow pool and depletion of labile SOC. These cycles also accelerated fast pool decay in modern soils and erosional transects, whereas burial dampened variability in Brady soils. Although continuous wetting increased overall decay in burial transects during the incubation period, wet–dry cycles destabilized the slow pool, which may result in greater long-term SOC loss. Together, these results underscore the importance of burial depth, geomorphic context, and moisture regime in shaping the long-term vulnerability of ancient SOC under climate change.

20 Summary

Buried ancient topsoils (Brady paleosol, Nebraska) sequester vast SOC. We found repeated drying/rewetting causes greater C loss than continuous wetting, destabilizing the slow-cycling C pool, especially in shallower soils. Decomposition rates are

0.4

¹Department of Life and Environmental Sciences, University of California, Merced, USA

²Department of Geography, University of Wisconsin–Madison, USA

³Department of Biological Sciences, Boise State University, USA





higher in erosional settings. Burial depth and moisture regime are key to the long-term vulnerability of these ancient C stocks under climate change.

5 1 Introduction

Global temperatures have risen by 1°C since the industrial era due to anthropogenic CO₂ emissions, confirming humandriven climate change (IPCC, 2018). Alongside warming, precipitation regimes are shifting - marked by increased frequency and intensity of wetting and drying events, especially in more arid ecosystems. These hydrologic fluctuations can destabilize long-stored soil organic carbon (SOC) by disrupting aggregates, increasing dissolution and solute mobility, and stimulating microbial decomposition (Berhe et al., 2012; Min et al., 2020; Hicks Pries et al., 2023). While limiting warming to below 2°C remains critical, mitigation via emissions reductions alone may be insufficient. Preserving or enhancing terrestrial carbon sinks, especially soils, offers a complementary pathway for climate stabilization.

While many studies examine topsoil carbon dynamics, whole-soil responses to changes in climate have rarely been tested (Hicks Pries et al., 2017). Subsoils hold nearly half of global SOC stocks (Jobbagy and Jackson, 2000) and this deep-soil carbon may be more sensitive to varying environmental conditions than surface soil (Min et al., 2020). Organic inputs reach subsoils via leaching of dissolved organic carbon and vertical transport of litter by bioturbation. SOC in deeper horizons typically features low carbon to nitrogen (C:N) ratios and long mean residence times, suggesting advanced microbial processing and relative stability (Rumpel and Kögel-Knabner, 2011). In contrast, topsoils buried by aeolian or alluvial deposition often retain legacy carbon signatures reflecting past vegetation and climate (Marin-Spiotta et al., 2014), diverging from modern surface soils. These buried soils have historically been isolated from near-surface conditions, including temperature and moisture fluctuations. Previous research supports this isolation effect: for instance, Chaopricha (2013) found negligible CO₂ fluxes from Brady Soil collected from 4 m below the modern surface when no water was added, indicating extremely limited microbial activity under such dry, oxygen-poor conditions.

Subsurface environments typically have limited oxygen, C inputs, and water availability, all of which constrain microbial activity and promote long-term SOC persistence (Soong et al., 2021). However, this protection may be compromised under climate change scenarios involving increased rainfall, warming, and surface disturbance (Fontaine et al., 2007; Gao et al., 2020; Hicks Pries et al., 2023). While burial isolates SOM from decomposers, enhancing its stability (Berhe et al., 2007; Stacy et al., 2015; Berhe et al., 2008), soil erosion, root intrusion, and hydrologic shifts can re-expose previously protected SOM. Erosion may also replace eroded C with increased photosynthate additions due to rejuvenation of rock-derived nutrients (Berhe et al., 2018). Given the global extent of geomorphic disturbance and the potential for reactivated decomposition, buried soils may represent an extensive but under-characterized carbon pool whose long-term persistence is uncertain (Chaopricha and Marín-Spiotta, 2014; Szymanski, 2021; Pal et al., 2023).

SOM decomposition is mediated by geomorphic and geochemical controls. Soil texture, mineralogy, and ionic composition shape organo-mineral associations and influence microbial access. Thermal transformation of buried SOM into condensed aromatic compounds can also increase resistance to decomposition (Marin-Spiotta et al., 2011; Schmidt et al., 2011). Recent



60

65

75



findings from Dolui et al. (in press) link persistent SOM turnover in buried soils to fine textures, higher conductivity, and enhanced organo-mineral bonding. These stabilizing mechanisms weaken with erosional exposure to surface conditions (soil moisture and oxygen) and priming of previously-stable SOM due to the introduction of fresh organic matter inputs (McMurtry et al., 2024), making SOM more vulnerable to loss.

Soil moisture dynamics are central to SOM persistence. Wetting and drying–rewetting cycles can destabilize aggregates, increase dissolved organic carbon leaching, and stimulate mineral-associated OM loss (Berhe et al., 2012; Neff and Asner, 2001; Li et al., 2023). Moisture influences microbial processes by modulating water potential, oxygen diffusion, and solute transport (Chowdhury et al., 2011; Davidson et al., 2012). Texture controls water retention during drying, while aggregate structure governs accessibility under saturated conditions (Or and Tuller, 1999; Ghezzehei et al., 2019).

In surface soils, especially in semi-arid and Mediterranean systems, drying—rewetting cycles produce strong mineralization pulses (Miller et al., 2005; Zhu and Cheng, 2013). Such cycles break down aggregates and release labile SOM, stimulating priming effects (Najera et al., 2020). Soils with broader pore-size distributions may retain water longer, sustaining microbial activity and potentially increasing cumulative SOM loss (Goebel et al., 2005). The effects of increased rainfall also depend on seasonal timing; for instance, winter precipitation can enhance subsoil C storage more than spring rain due to deeper translocation of carbon (Wahab et al., 2025).

As soils dry, physical and chemical processes can strengthen OM-mineral interactions. Solute precipitation, matric tension, and shifts toward stronger bonding (e.g., inner-sphere complexes) promote greater SOM-mineral affinity (Kaiser et al., 2015; Kemper et al., 1987; Kang and Xing, 2008). Reorientation of amphiphilic compounds on mineral surfaces can increase hydrophobicity (Horne and McIntosh, 2000), potentially misleading assessments of SOM stability under drier conditions.

CO₂ efflux in subsoils is shaped by physical constraints - lower porosity, higher bulk density, and greater water-filled pore space - which suppress microbial respiration after rewetting (Min et al., 2020; Hill et al., 1985; Beare et al., 2009; Schrumpf et al., 2013). Subsurface microbial communities are often dominated by drought-tolerant fungi (Bird and Torn, 2006), and experience fewer moisture and temperature fluctuations than surface soils (Rumpel and Kögel-Knabner, 2011). Microbial "resistance" to drying manifests as reduced respiration during dry-down, while "resilience" describes rapid respiration rebound after rewetting (Leizeaga et al., 2021; Griffiths and Philippot, 2013). Soils with frequent drying–rewetting history tend to support more resilient microbial communities (Fierer and Schimel, 2003; Steenwerth et al., 2005).

In semi-arid systems, soil inorganic carbon (SIC) also contributes to carbon dynamics. SIC accumulates at depth through carbonate dissolution–precipitation cycles (Sharififar et al., 2023; Batool et al., 2024; Cotrufo and Lavallee, 2025). This is seen in the Brady Soil, a late Pleistocene paleosol buried by loess ca. 13,000–10,000 years ago in the Great Plains of the US (Jacobs and Mason, 2007; McDowell, 2020). SIC interacts with SOC via aggregation and mineral associations but can be mobilized through leaching under increased moisture conditions (Naorem et al., 2022; Liu et al., 2018; Tsypin and Macpherson, 2012).

Despite growing interest in buried SOM, moisture-driven decomposition patterns across landforms remain unclear. This study investigates the sensitivity of modern and buried SOM to moisture inputs under erosional and depositional geomorphic conditions in the Brady Soil. According to the U.S. National Climate Assessment (2018), the Central Great Plains region of





Nebraska is projected to warm by 3.5–9.5°C, with annual precipitation increasing by 2.5 cm. Erosion driven by agriculture, grazing, wind, and rainfall threatens to re-expose buried SOM to surface conditions.

We conducted a laboratory incubation using soils collected near Wauneta, Nebraska, to compare CO₂ efflux under continuous wetting versus drying—rewetting regimes. The area's semi-arid climate with seasonal moisture variability provides a relevant setting to test SOM responses to hydrologic fluctuations. Our hypotheses were: (i) Brady SOM is more stable and decomposes more slowly than modern SOM as reduced moisture and oxygen availability limit decomposition of SOM due to isolation from the soil surface; (ii) buried SOM in erosional settings is more vulnerable to loss due to exposure of previously protected SOM to surface conditions and mixing with modern carbon; and (iii) wetting will stimulate CO₂ release from previously buried soils as a result of increased substrate availability due to enhanced dissolution, solute transport, microbial decomposition, and/or aggregate disruption. By evaluating the interactions between moisture, geomorphology, and SOM dynamics, we aim to improve predictions of carbon stability under future climate and land-use change.

2 Methods and materials

2.1 Site and sampling

100

105

110

115

120

The field site is situated near Wauneta, within the loess tablelands of southeastern Nebraska, USA (40°29'52.8" N, 101°24'36" W; see Fig. 1). The region experienced reduced loess input during the terminal Pleistocene and early Holocene (13–10 ka) that permitted soil formation, leading to the development of the Brady Soil. Subsequent aridification renewed dust flux, resulting in its burial by younger loess (Johnson et al., 2007; Mason et al., 2008). Additional loess accumulation throughout the Holocene preserved weaker paleosols formed during intermittent depositional pauses (Mason et al., 2003; Miao et al., 2007). Recognized as a key paleoenvironmental and stratigraphic unit, the Brady Soil is regionally traceable across Nebraska, northeastern Colorado, and northern Kansas (Johnson and Willey, 2000).

The area is characterized by broad, flat uplands and sharply incised edges, providing natural windows into stratified soil profiles. Loess cover above the Brady Soil tapers in a downwind direction across the summits where it is thickest, producing burial transects of variable thickness. The local climate is semi-arid, with an average annual temperature of 9.7°C and ca. 495 mm of precipitation, concentrated during the summer months, with occasional snow in winter. Natural vegetation includes a mix of C3 and C4 grasses, replaced by cropland on many level surfaces today, but remaining at the study site and on steeper terrain in general.

Brady Soil exposures are visible in actively eroding margins, gullies, and roadside cuts. Prior investigations, including coring and field surveys, confirm its continuity beneath the summit landform (Jacobs and Mason, 2004; Marin-Spiotta et al., 2014; Mason et al., 2008). Surface soils developed in Holocene loess are weakly developed and light-colored, typically classified as Mollisols, Inceptisols, or Entisols. Although different in age, modern and buried soils share similar parent material and mineralogy due to the region's limited weathering intensity. Brady A horizons (Ab) are identified by their dark grayish brown coloration (Munsell 10YR3/2 to 10YR4/2) and silt loam texture, generally overlying Bk or Bw horizons (Szymanski, 2021; Jacobs and Mason, 2007; McDowell, 2020).





Sampling was conducted in 2016 and 2017 across both burial and erosional settings, targeting the Brady Soil and its overlying counterparts. We collected samples at three depths from each of three replicate transects per setting (details in Fig. 1). Burial transects encompassed sites with differing overlying loess thickness, while erosional transects followed slope gradients with varying degrees of Brady Soil exhumation through erosion. Samples were retrieved from two intervals (0–30 cm and 30–60 cm, adjusted for shallower profiles when necessary). A Giddings probe (10.2 or 8.9 cm diameter) with plastic liners was used for intact sampling in burial settings, while soil pits were dug for erosional profiles. Sampling stratigraphy relative to the present land surface was categorized using Roman numerals (Table A1); complete methods are described in (Szymanski, 2021).

2.2 Soil chemical and physical analyses

General soil physical and chemical properties were determined by standard soil analytical methods, as described in detail in Dolui et al. (in press) and Szymanski (2021). Briefly, soil pH and electrical conductivity (EC) of soil samples were determined in 1: 2 water extracts. Total soil C, TOC and TIC content were determined by combustion using an elemental analyzer with an intermediate acidification step to remove carbonates. Exchangeable base cation concentrations (Ca^{2+} , Mg^{2+} , Na^+ and K^+) were determined by the ammonium acetate extraction method (buffered to pH 7) followed by quantitative analysis using ICP-OES. Sodium adsorption ratio (SAR) was determined by dividing concentration of Na in soil extract by the square root of half of sum of Ca and Mg concentrations (Dolui et al., in press). Particle size distribution was determined using the pipette method for clay content and laser diffraction for silt and sand content Szymanski (2021). Radiocarbon (^{14}C) analyses of bulk soil samples were conducted to determine the age and turnover time of carbon in both modern and buried soils. Samples were pre-treated, combusted, and then measured using accelerator mass spectrometry (AMS). The $\Delta^{14}C$ results were used in a homogeneous, open-system, steady-state soil carbon decomposition model to estimate carbon turnover times (Dolui et al. (in press)) which were averaged for the three replicate transects.

2.3 Incubation experiments

The incubation experiment was set up to determine the effect of continuous wetting and drying-rewetting on SOC fluxes using soils that were collected from the upper surface (0–30 cm) of modern soils and the upper layer (0–30 cm) of Brady Soil samples at depositional and erosional transect types. All soils were passed through a 2 mm sieve, homogenized, and subsampled for incubation experiments. Two types of water addition experiments were conducted: continuous wet and drying-rewetting. To isolate the effects of moisture, roots >2 mm were removed by sieving and manual sorting.

2.3.1 Experimental setup

The incubation experiments were conducted in 8 oz mason jars. The treatments included (i) continuous wet – soils maintained at 60% water holding capacity (WHC) throughout the experiment and (ii) drying–rewetting cycles – soils were dried for 7 days, then rewetted to 60% WHC (for 8 cycles). Each treatment had two replicates (subsamples derived from a single composite of



155

170



replicate transects per soil type), and control soils were maintained at 5% WHC. The total incubation time was 225 days for the continuous wet treatment and 56 days for the drying–rewetting treatment.

Previously homogenized soils were sub-sampled and added to jars at an equivalent of 30 ± 0.5 g dry mass. After adding a predetermined amount of ultra-pure Milli-Q water, the jars were kept at room temperature (ca. 25°C), matching the average summer soil temperature (when most precipitation occurs) at the site (UNL Soil Temperature Data). Jars were sealed with lids fitted with rubber septa for headspace gas collection, and silicone gel was applied around the septa to prevent gas leakage.

In the continuous wet experiment, soils were maintained at 60% WHC and sealed until sampling. On average, water loss was 0.01 mL/day, ranging from 0.005 to 0.02 mL/day. Water was added after gas sampling to avoid inducing the Birch effect. After each sampling, lids were left open for one hour to allow CO₂ equilibration with ambient air.

In the drying–rewetting experiment, soils were rewetted every 7 days by slowly adding Milli-Q water to reach 60% WHC. After water addition, jars were sealed, and headspace gas was sampled 6 hours later to capture Birch effect emissions. Soils were then dried to 5% WHC by removing the lids and incubating at ca. 25°C.

55 2.3.2 Sampling schedule and CO₂ analysis

In the continuous wet experiment, headspace gas samples for CO₂ analysis were collected on days 1, 3, 5, 7, 11, 16, 27, 55, 82, 114, 151, and 225. After each sampling, jar lids were opened for one hour to equilibrate with ambient air.

In the drying–rewetting experiment, jars were sealed for 6 hours after water addition, and headspace gas was sampled on days 1, 7, 21, 28, 35, 42, and 49 to evaluate the Birch effect. Control samples were collected on the same days for both experiments. Evolved CO₂ concentrations were analyzed using a Shimadzu 2014 gas chromatograph (Kyoto, Japan) with a thermal conductivity detector at UC Merced and an LI-830 infrared gas analyzer (IRGA) at Lawrence Livermore National Laboratory (LLNL).

2.4 Statistical analyses

Statistical analyses were performed using CRAN-R 4.5.0 (R Core Team, 2025). Soil-respired CO₂ measurements from the incubation experiment were averaged over two sample replicates for treatments, while the control was only representative of a single value. The concentration of soil respired CO₂ was expressed as the mass of C per mass of SOC, as follows:

$$\mu g C - CO_2 g soil C^{-1} = mmol air \times \frac{\mu mol CO_2}{mol air} \times \frac{10^{-3} mol air}{mmol air} \times \frac{12 \mu g C}{\mu mol C} \times \frac{1}{g TOC}$$
(1)

For the continuously wet experiments, we calculated cumulative respiration flux by summing continuous wet fluxes throughout the incubation for the continuous wetting experiment (225 days). Two-pool first-order decay models were fitted according to the equation:



185

190

200

205

210



$$\mathbf{C_{CO_2}}(t) = C_0 \left(1 - (f_f e^{-k_f t} + f_s e^{-k_s t}) \right)$$
 (2)

where C_{CO_2} (t) is the cumulative mass of C (μ g) lost via respiration by the incubated soil at day t, C_0 denotes TOC, $f_f + f_s = 1$ denote the fast and slow cycling fractions of the TOC, respectively and k_f and k_s are the corresponding decay rate constants. The model was fitted to the data with a non-linear least-squares fitting function using the minpack.lm package in R (Elzhov et al., 2023).

For the wet-dry cycling experiment, we calculated cumulative respiration flux by summing fluxes over wetting periods (assuming negligible flux over drying periods; Chaopricha (2013)) for the duration of the experiment (49 days). Two-pool first-order decay models were fitted similarly to the procedure followed for the continuously wet experiment, but the day (t) was approximated from the cumulative sum of wetting periods only (total of 2 days).

Preliminary modeling showed that the proportion of slow- versus fast-cycling SOM pools in the wet-dry cycling experiment was 0.999: 0.001, indicating that the wet-dry cycling decay model was representative of a homogeneous (one-pool) system, dominated by this "slow" pool. Therefore, for both continuously wet and wet-dry cycling experiments, we also fitted one-pool first-order decay models using non-linear least-squares optimization, according to the equation:

$$\mathbf{C_{CO_2}}: (t) = C_0 (1 - e^{-kt})$$
 (3)

where k is the single-pool first-order decomposition rate constant.

The effects of transect type, paleostatus, degree of burial or exposure and their interactions on soil organic matter decay rates and fraction sizes during incubations were tested by generating linear mixed-effects models treating replicates as a random effect (excluding controls), using the packages nlme (Pinheiro et al., 2024) and emmeans (Lenth, 2024). Significant differences across factor levels and interactions were evaluated by calculating pairwise Sidak tests. We also tested effects of transect type, paleostatus and degree of burial/ exposure on day-1 CO₂ pulses of the wet-dry incubation experiment.

We compared the total CO_2 loss from the 49 days of wetting in the wet-dry incubations to the modeled CO_2 loss over 49 days in the continuously wet experiment. We used a linear mixed-effects model to analyze the treatment groups. The model's fixed effects were Paleostatus, transect type, and Depth, and their interactions. We treated replicates as a random effect. We then used marginal means and pairwise comparisons to compare the wet-dry and continuously wet experiments. For the control samples, we used a similar model but with Paleostatus and transect type as the only fixed effects and Depth as a random effect. We performed pairwise comparisons to analyze the effects of paleostatus, transect type, and their interaction.

The mean cumulative CO_2 losses of controls vs treatments were compared by a Welch test after establishing unequal variance of the datasets using the Bartlett test, using the stats package (RStudio Team, 2019). A linear mixed-effects analysis was also performed to evaluate the effects of transect type and paleostatus on cumulative CO_2 losses of the control samples. Due to the absence of replication, depth was treated as a random effect.

Multiple linear regression (MLR) was used to estimate the size of the effect of soil physicochemical properties (soil pH, EC, TOC and TIC content, SAR, textural composition and exchangeable base cation concentrations) on the decomposition rates



215

220

225

230



of the fast and slow pools and fraction size of the slow pool, as modeled from the continuous wetting incubation experiment. The size of soil physicochemical property effects on the decomposition rate of SOM derived from a one-pool model was estimated for the wet-dry cycling experiment. We developed models using stepwise regression, proceeding in both forward and backward directions with the stats package (R Core Team, 2025). Model selection prioritized parsimony, which was evaluated through the Akaike Information Criterion (AIC), as implemented in the MASS package (Venables and Ripley, 2002). The coefficient, intercept, R², and root mean squared error (RMSE) for each model were subsequently computed using the stats package (R Core Team, 2025). A matrix displaying pairwise Pearson correlation coefficients and their significance levels was also generated to visualize the relationships between soil physicochemical properties and the modeled SOM decomposition parameters, using the stats and ggplot2 packages (RStudio Team, 2019).

3 Results

3.1 General soil properties

The physicochemical properties of soils used in the incubation experiment are shown in Table 1. The soils were relatively alkaline (pH ranging from 6.89 to 7.77), especially the Brady Soil. The clay, silt and sand content placed the soils in the texture class category of silt loam. Total organic carbon was higher in modern soils due to active biomass inputs, while inorganic carbon content was higher in the Brady Soil due to carbonate formation (cite Dolui et al i.e. paper 1). The Brady soil of the burial transect was classified as saline (mean EC of 5.41 dS m⁻¹) and the CEC of soils was moderately high, ranging from 15.17 - 23.31 and indicating the presence of higher activity clays. The turnover time of bulk soils as derived from radiocarbon-based models, was much greater in the Brady Soil (8327 - 15 654 years) compared to modern soils (576.4 - 1451 years), confirming the long-term stability of SOM in the paleosol (cite Dolui et al. i.e., paper 1). The mean CN ratio in both Brady and modern soils was relatively low (ca. 10), indicating a sufficient supply of N for plant growth and microbial activity.

3.2 Effects of continuous wetting on soil CO₂ efflux

Cumulative C lost from soils via respiration of CO_2 during the continuously wet incubation are shown in Fig. 2. Raw incubation data and figures of merit of statistical comparative tests are available online at DOI: doi: 10.17632/fjw646gpyf.1.

In the continuous wet soil treatment group, modern soils evolved significantly higher CO_2 (mean of 30.6 mg CO_2 -C g C^{-1}) compared to Brady Soil (mean of 15.9 \pm 2.39 mg CO_2 -C g C^{-1}) after 225 days of incubation (p <0.01). Soils of the erosional transect type had greater cumulative C loss (mean of 29.3 mg CO_2 -C g C^{-1}) compared to the depositional transect (mean of 17.3 \pm 2.39 mg CO_2 -C g C^{-1} , p < 0.01). However, the difference between cumulative C losses of erosional vs depositional transect types was not significant at the greatest depth.

Modern soil in the erosional transect had significantly higher cumulative C losses (mean of 35.9 mg CO_2 -C g C^{-1}) than modern soil of the depositional transect (mean of 25.3 mg CO_2 -C g C^{-1} , p < 0.05). Similarly, Brady Soil of the erosional



255

260

270



transect had significantly higher cumulative C losses (mean of 22.6 mg CO_2 -C g C^{-1}) compared to the depositional transect (mean of 9.28 mg CO_2 -C g C^{-1} , p < 0.05).

The Brady soil with an intermediate degree of erosion had higher cumulative CO_2 loss (mean of 33.2 mg CO_2 -C g C^{-1}) compared to Brady Soil of other depths, while the Brady soil with the greatest degree of burial had the lowest cumulative CO_2 loss (mean of 4.14 mg CO_2 -C g C^{-1} , differences not significant). For Brady soil of the depositional transect, the magnitude of cumulative CO_2 efflux among different depths was in the order of shallowest > intermediate > deepest, whereas in the erosional transect, the order was intermediate > shallowest > deepest.

The cumulative CO_2 evolution of 60% WHC continuous wet experiments (mean of 23.3 mg CO_2 -C g C^{-1}) was significantly greater than control soils maintained at 5% WHC (mean of 0.478 mg CO_2 -C g C^{-1} , p < 0.001). Among the control soils, Brady Soil of the depositional transect had significantly greater C losses (mean of 0.561 mg CO_2 -C g C^{-1}) compared to modern soils (mean of 0.253 \pm 0.0683 mg CO_2 -C g C^{-1} , p < 0.05), but C losses in modern and Brady Soil were more similar in the erosional transect (mean of 0.254 and 0.444 mg CO_2 -C g C^{-1} for modern and Brady Soil respectively, n.s.).

Significance of differences in cumulative CO₂ losses among degree of burial/ exposure for control samples could not be tested due to lack of replication, but we report observed differences. Among the depositional transect control soils, the shallowest depth Brady soil produced the greatest cumulative CO₂ loss, while modern soil collected from the intermediate degree of burial soil produced the least cumulative CO₂ loss. Among the erosional transect control soils, the most CO₂ was evolved in the intermediate depth Brady soils, and the lowest CO₂ was evolved in the modern soil collected from the lowest degree of burial.

3.3 Effect of drying and rewetting on soil CO₂ efflux

Daily C lost from soils via respiration of CO_2 during the dry-rewetting incubation are shown in Fig. A1 and cumulative C losses are shown in Fig. 3. Soil respiration data from the dry-rewetting incubation are available online at DOI: doi: 10.17632/fjw646gpyf.1.

The largest respiration fluxes were produced on the first day, with significantly greater cumulative CO_2 loss from modern soils (mean of 0.920 mg CO_2 -C g C^{-1}) compared to Brady Soil (mean of 0.729 \pm 0.034 mg CO_2 -C g C^{-1} , p < 0.01), but the reverse was observed at the greatest depth. Respiration pulses declined over time for all soils. Control soils had a lower day ⁻¹ pulse CO_2 (mean of 0.295 mg CO_2 -C g C^{-1}) compared to the dry-rewetting treatment (mean of 0.824 mg CO_2 -C g C^{-1} , p < 0.001), but there was no significant difference between the cumulative CO_2 loss from control (21.9 mg CO_2 -C g C^{-1}) and treatments (17.5 mg CO_2 -C g C^{-1}) by the final day of incubation.

After 49 days of incubation under wet-dry cycles, the Brady Soil from both the burial and the erosional transects emitted significantly more cumulative CO_2 (0.0183 g CO_2 -C g C^{-1}) than Brady Soil incubated under continuously wet conditions (0.009 \pm 0.0005 g CO_2 -C g C^{-1} , p < 0.001). However, there was no significant difference between cumulative CO_2 loss in modern soils incubated under wet-dry cycles versus continuous wet conditions.

The order of magnitude of total CO_2 emission after 49 days followed the order erosional modern > erosional Brady > depositional modern > depositional Brady. Soils of the erosional transect (mean of 18.3 mg CO_2 -C g C^{-1}) had significantly greater cumulative CO_2 loss compared to the depositional transect (mean of 16.7 \pm 0.643 mg CO_2 -C g C^{-1} , p < 0.01). Modern



280

285

300

305



soil had significantly greater cumulative CO_2 loss (mean of 16.7 mg CO_2 -C g C^{-1}) than Brady Soil (mean of 18.3 \pm 0.390 mg CO_2 -C g C^{-1} , p < 0.001), but the difference was not significant at the intermediate depth. Modern soil from the shallowest depth emitted significantly more cumulative CO_2 (19.2 mg CO_2 -C g C^{-1}) than the deepest layer (13.9 mg CO_2 -C g C^{-1} , p < 0.05). However, the opposite was observed in Brady Soil, where the deepest layer emitted more cumulative CO_2 (15.6 mg CO_2 -C g C^{-1}) compared to the shallowest layer (20.4 mg CO_2 -C g C^{-1} , p < 0.05). Among the control soils, although Brady Soil emitted more cumulative CO_2 than modern soil, there was no significant difference. This was likely due to large variation of the depth-pooled samples (in absence of control replicates), as a result of the much larger CO_2 loss from Brady Soil of the erosional transect at the greatest depth compared to other samples.

3.4 Decay rates and fraction sizes of soil organic matter pools

The decomposition rate of the slow pool and size of the fast pool under continuous wetting is shown in Fig. 4 and the decomposition rate of SOM (single pool) under wet-dry cycles is shown in Fig. 5. Statistical Figures of merit of linear mixed-effects models are available online at DOI: doi: 10.17632/fjw646gpyf.1.

The slow-cycling SOM pool under continuous wetting decayed ca. 2000 times more slowly than the fast-cycling pool, with a significantly lower mean decay rate in the burial transect $(8.68 \cdot 10^{-6} \text{ day}^{-1} \text{ i.e.}, 315 \text{ years turnover time, henceforth referred to as TOT) compared to the erosional transect <math>(1.36 \cdot 10^{-5} \pm 6.82 \cdot 10^{-7} \text{ day}^{-1} \text{ i.e.}, 201 \text{ years TOT, p} < 0.01)$. Thus, higher decay rates correspond to faster (shorter) turnover times throughout this section. The mean decay rate of the slow-cycling SOM pool of Brady Soil $(6.86 \cdot 10^{-6} \text{ day}^{-1} \text{ i.e.}, 399 \text{ years TOT})$ was significantly lower than that of modern soil $(1.54 \cdot 10^{-5} \text{ day}^{-1} \pm 6.82 \cdot 10^{-7}, \text{ i.e., } 178 \text{ years TOT, p} < 0.001)$. The mean decay rate of the slow-cycling SOM pool of modern soil in the burial transect was significantly greater at the greatest degree of burial $(1.53 \cdot 10^{-5} \text{ day}^{-1} \text{ i.e., } 178 \text{ years TOT})$, compared to the lowest degree of burial $(9.97 \cdot 10^{-6} \text{ day}^{-1} \text{ i.e., } 275 \text{ years TOT, p} < 0.05)$.

The mean decay rate of the fast-cycling SOM pool of the erosional transect (0.130 day⁻¹ i.e., 7.68 days TOT) under continuous wetting was significantly higher (i.e., faster turnover) than that of the burial transect (0.126 \pm 0.001 day⁻¹ i.e., 7.96 days TOT, p < 0.05). The mean decay rate of the fast-cycling SOM pool of Brady Soil in the erosional transect was significantly greater at the greatest degree of erosion (0.144 day⁻¹ i.e., 6.96 days TOT) compared to the lowest degree of erosion (0.121 day⁻¹ i.e., 8.25 days TOT, p < 0.01).

The decay rate of SOM (one-pool model) under wet-dry cycles did not differ significantly among soils of different paleostatus or transect type. In the two-pool model, the decay rate of the slow-cycling SOM pool under wet-dry cycles was significantly higher in the erosional transect (0.007 day⁻¹ i.e., 129 days TOT) compared to the burial transect (0.009 \pm .0002 day⁻¹ i.e., 117 days TOT, p < 0.05), indicating faster SOM turnover where decay rates were higher. The decay rate of the fast-cycling SOM pool in the burial transect was significantly higher in modern soil (8.11 \pm 1.94 day⁻¹ i.e., 0.123 days TOT) compared to Brady soil (0.558 day⁻¹ i.e., 1.79 days TOT).

The slow-cycling pools of both modern and Brady Soil under continuous wetting contained a much greater proportion of total SOC (> 96%) than the fast-cycling pool. The fraction size of the fast-cycling pool relative to the slow-cycling pool under continuous wetting was significantly greater in the erosional transect (0.014) compared to the burial transect (0.012 \pm 0.0003,



320



p < 0.01) and significantly greater in modern soils (0.0173) compared to Brady Soil (0.009 \pm 0.0003, p < 0.001). The fraction size of the fast and slow pools tended to 0 and 1.0 respectively in all soils under wet-dry cycling, nullifying the statistical comparison results among soils of different paleostatus and transect types.

3.5 Decay rates and fraction sizes of soil organic matter pools in continuous wet versus wet-dry experiment

A summary of SOM decomposition model parameters (one-pool and two-pool) of the continuously wet and wet-dry cycling experiments is shown in Table 2. Statistical figures of merit of linear mixed-effects models are available online at DOI: doi: 10.17632/fjw646gpyf.1.

With the one-pool models, the continuously wet soils had a significantly higher decay rate $(0.00865 \text{ day}^{-1} \text{ i.e.}, 116 \text{ days} \text{ TOT})$ compared to the wet-dry cycles $(0.00714 \text{ day}^{-1} \text{ i.e.}, 140 \text{ days} \text{ TOT}, p < 0.01)$, indicating faster turnover under continuous wetting. In the burial transect, the one-pool decay constant of the continuous wet experiment was significantly higher $(0.0103 \text{ day}^{-1} \text{ i.e.}, 97.4 \text{ days} \text{ TOT})$ than that of the wet-dry cycling experiment $(0.00690 \text{ day}^{-1} \text{ i.e.}, 145 \text{ days} \text{ TOT}, p < 0.001)$. However, there was no significant difference between the decay constant of the continuous wet and wet-dry experiments in erosional transects. These trends were observed in both Brady and modern soils.

Among the control soils with one-pool models, the continuous wet experiment had a significantly higher decay rate (0.0376 day⁻¹ i.e., 26.6 days TOT) compared to the wet-dry cycling experiment (0.00146 day⁻¹ i.e., 179 days TOT, p < 0.001), again meaning faster decomposition under continuous wetting. This was true in both burial (continuous wet k = 0.0374 day⁻¹ i.e., 26.7 days TOT and wet-dry k = 0.00372 i.e., 268 days TOT) and erosional (k = 0.0377 day⁻¹ i.e., 26.5 days TOT and wet-dry k = 0.00746 day⁻¹ i.e., 134 days TOT) transects, as well as Brady (continuous wet k = 0.0376 day⁻¹ i.e., 26.6 days TOT and wet-dry k = 0.00871 day⁻¹ i.e., 115 days TOT) and modern (continuous wet k = 0.0375 day⁻¹ i.e., 26.7 days TOT and wet-dry k = 0.00248 day⁻¹ i.e., 404 days TOT) soils.

With the two-pool models, the decay rate of the slow-cycling SOM pool in the continuously wet experiment was significantly lower (1.11 \cdot 10⁻⁵ day⁻¹ i.e., 246 years TOT) than that of the wet-dry cycling experiment (0.00812 day⁻¹ i.e., 123 days TOT, p < 0.001), reflecting faster turnover in the wet-dry treatments. This was true in both Brady (continuously wet k = 6.86 \cdot 10⁻⁶ day⁻¹ i.e., 399 years TOT, wet-dry k = 0.0083 day⁻¹ i.e., 120 days TOT) and modern (continuously wet k = 1.54 \cdot 10⁻⁵ day⁻¹ i.e., 178 years TOT, wet-dry k = 0.00793 day⁻¹ i.e., 126 days TOT) soils, as well as both burial (continuously wet k = 8.68 \cdot 10⁻⁶ day⁻¹ i.e., 316 years TOT, wet-dry k = 0.00773 day⁻¹ i.e., 129 days TOT) and erosional (continuously wet k = 1.36 \cdot 10⁻⁵ day⁻¹ i.e., 202 years TOT, wet-dry k = 0.0085 day⁻¹ i.e., 118 days TOT) transects, and in all depth layers.

The decay rate of the fast-cycling SOM pool in modern soil was significantly higher in the wet-dry cycling experiment (8.11 day⁻¹ i.e., 0.123 days TOT) compared to the continuously wet experiment (0.127 day⁻¹ i.e., 7.89 days TOT, p < 0.001), indicating a much faster turnover response to rewetting. The decay rate of the fast-cycling pool in the erosional transect was also significantly higher in the wet-dry cycling experiment (5.148 day⁻¹ i.e., 0.194 days TOT) compared to the continuously wet experiment (0.130 day⁻¹ i.e., 7.68 days TOT). Separating these effects by depth revealed that the significance of the difference between the fast pool decay rate in modern soils was more evident at the intermediate and greatest depth. The decay



365



rate of the fast-cycling SOM pool did not differ significantly between continuously wet and wet-dry cycling experiments in Brady soils or in the burial transect.

Among the control soils with two-pool models, the continuous wet experiment had significantly lower slow pool decay rate $(1 \cdot 10^{-8} \text{ day}^{-1} \text{ i.e.}, 274\,000 \text{ years TOT})$ compared to the wet-dry cycling experiment (k = 0.005 day⁻¹ i.e., 200 days TOT, p < 0.01), again corresponding to much faster turnover in the wet-dry treatments. This was true in both the burial and erosional transects, modern and Brady Soil and at all depths.

The decay rate of the fast-cycling SOM pool of control Brady Soil was significantly higher in the wet-dry cycling experiment (0.0556 day⁻¹ i.e., 18.0 days TOT) compared to the continuously wet experiment (10.3 day⁻¹ i.e., 0.0971 days TOT). This was true in both burial and erosional transects. In modern soils, however, there was no significant difference between decay rates of fast-cycling SOM in continuously wet versus wet-dry cycling experiments.

The fraction size of the slow-cycling SOM pool in the wet-dry cycling experiment was significantly larger (0.999) than that of the continuously wet experiment (0.987, p < 0.001) - this was true for both Brady and modern soils, across erosional and burial transects and at all depths. It follows that the fraction size of the fast-cycling SOM pool in wet-dry cycling experiments was significantly smaller (0.001) than that of the continuously wet experiment (0.0131, p < 0.001) for soils of all transect types, paleostatus groups and depth categories. There was no significantly difference between fraction sizes of the slow-cycling SOM pool among the controls of the wet-dry cycling and continuously wet experiment; the fast-cycling pool was also similar among control soils of the two experiments.

3.6 Relationships between soil properties and carbon dynamics

The true versus predicted values MLR models for prediction of decomposition rates of the fast- and slow-cycling pools as well as the fraction size of the slow pool are shown in the Appendix, Fig. A2. A matrix showing the correlation between these variables is given in Fig. 6. The intercept, coefficients of explanatory variables, RMSE and R² of the best-performing MLR models, are given as follows.

$$\begin{aligned} \mathbf{k}_{\mathrm{slow}} &= 0.0000532 - 0.0000979 \cdot \mathrm{SAR} + 0.000000225 \cdot \mathrm{clay} + 0.000000395 \cdot \mathrm{Ca} \\ &- 0.00000622 \cdot \mathrm{Mg} - 0.00000271 \cdot \mathrm{K} + 0.00000347 \cdot \mathrm{EC} - 0.00000618 \cdot \mathrm{pH} \\ &- 0.00000687 \cdot \mathrm{TOC} - 0.0000275 \cdot \mathrm{TIC} \\ &\mathrm{RMSE} : 0.000000701, \quad \mathbf{R^2} : 0.98 \end{aligned}$$

(4)





(5)

(6)

(7)

$$\begin{aligned} \mathbf{k}_{\mathrm{fast}} &= 0.215 + 0.0189 \cdot \mathrm{SAR} + 0.00344 \cdot \mathrm{clay} + 0.0026 \cdot \mathrm{Ca} + 0.00204 \cdot \mathrm{Mg} \\ &- 0.000302 \cdot \mathrm{K} - 0.00513 \cdot \mathrm{EC} - 0.0196 \cdot \mathrm{pH} + 0.0146 \cdot \mathrm{TIC} \\ &\mathrm{RMSE} : 0.00141, \quad \mathbf{R^2} : 0.95 \end{aligned}$$

$$\begin{aligned} \mathbf{f}_{\mathrm{slow}} &= 0.976 + 0.0732 \cdot \mathrm{SAR} - 0.000362 \cdot \mathrm{clay} - 0.000241 \cdot \mathrm{Ca} + 0.00138 \cdot \mathrm{Mg} \\ &+ 0.00283 \cdot \mathrm{K} - 0.00288 \cdot \mathrm{EC} + 0.00174 \cdot \mathrm{pH} - 0.000707 \cdot \mathrm{TOC} \\ &+ 0.0298 \cdot \mathrm{TIC} \end{aligned}$$

RMSE: 0.000838, \mathbf{R}^2 : 0.97

$$\begin{aligned} \mathbf{f}_{\mathrm{fast}} &= 0.0243 - 0.0732 \cdot \mathrm{SAR} + 0.000362 \cdot \mathrm{clay} + 0.000241 \cdot \mathrm{Ca} - 0.00138 \cdot \mathrm{Mg} \\ &- 0.00283 \cdot \mathrm{K} + 0.00288 \cdot \mathrm{EC} - 0.00174 \cdot \mathrm{pH} + 0.000707 \cdot \mathrm{TOC} \end{aligned}$$

RMSE: 0.000838, $\mathbf{R}^2: 0.97$

 $-0.0298 \cdot TIC$

The MLR models for prediction of decay rates of SOM under continuous wetting had better model fit ($R^2 > 0.80$) compared to those for predictions of SOM pool fraction size ($R^2 = 0.44$). From the MLR equations, we deduce that soil properties with the greatest coefficients had the most important effects on the SOM decay rate and fraction size model parameters. While SAR increased the rate of decay and decreased the size of the of the slow pool, an opposite trend is observed in the fast pool.

TOC and pH also increased the decay rate of the fast-cycling SOM pool under continuous wetting, while the slow pool decay rate decreased with increasing TIC. TOC and TIC increased the fraction size of the slow pool at the expense of fraction size of the fast pool. When considering effects of these factors individually, SAR, TOC, TIC and pH did not have significant correlation





with SOM decomposition parameters (Fig. 6). However, exchangeable Mg and K content were significantly correlated with the decay rate of the fast (negative correlation) and slow (positive correlation) pools (Fig. 6).

The true versus predicted values MLR models for prediction of the decomposition rate of SOM (one-pool system) under wet-dry cycles are shown in the Appendix, Fig A3. A matrix showing the correlation between these variables is given in Appendix, Fig. A4.

The intercept, coefficients of explanatory variables, RMSE and R^2 of the best-performing MLR model for prediction of the decay rate, are given as follows.

$$\mathbf{k} = -0.00641 - 0.00308 \cdot \text{SAR} + 0.000599 \cdot \text{clay} - 0.000141 \cdot \text{Ca}$$
$$-0.0015 \cdot \text{Mg} + 0.00118 \cdot \text{K} + 0.00159 \cdot \text{pH}$$
$$+0.002 \cdot \text{TOC}$$

RMSE: 0.000215, \mathbf{R}^2 : 0.94

(8)

SAR decreased the decay rate of SOM under wet-dry cycles. Clay and TOC content increased the decay rate of SOM. Exchangeable Ca, Mg content decreased the decay rates of both pools. Considering these parameters individually (correlation coefficients) revealed a weak correlation with k. Therefore MLR, where k is modeled as a function of all predictors together, demonstrates that the combination of these variables explained most variance, while no single predictor explained much variance on its own.

390 4 Discussion

395

4.1 Stabilization of soil organic matter by burial

Brady Soil under continuous wetting exhibited lower cumulative CO_2 evolution compared to modern soils across both erosional and depositional transects (Fig. 2 and Appendix, Fig. 3). This enhanced stability may be attributed to several mechanisms: flocculation facilitated by polyvalent cations such as Ca^{2+} (Dolui et al., in press), the abundance of pyrogenic SOM (Marin-Spiotta et al., 2014; Schmidt et al., 2011), and strong organo-mineral associations (Szymanski, 2021).

The slightly larger relative size of the fast-cycling SOM pool in modern soils compared to Brady Soil may reflect recent inputs. Direct comparison of decay rates of SOM pools in modern versus Brady Soil reveals a marked difference in SOM persistence (Fig. 4). Notably, the slow-cycling pool in Brady soils from the most eroded transect exhibited significantly lower decay rates under continuously wet incubation than its modern counterpart - clear evidence of greater SOM persistence in the



410

415

420

430



paleosol. Across treatments, the slow pool decayed roughly 2000 times more slowly than the fast pool, with Brady soils showing TOTs of 399 years compared to 178 years TOT in modern soils. The multiple linear regression (MLR) equations showed a negative relationship between the slow pool decay rate (k_{slow}) and total inorganic carbon (TIC) as well as exchangeable Mg²⁺ content (Equation 4). While CaCO₃ cementation was not pronounced, the positive correlations between TOC, TIC, and Ca in Brady soils from erosional transects (Dolui et al., in press) - where shallow wetting promotes near-surface carbonate precipitation - suggests a stabilization role for carbonate phases.

The Brady soils also contained more fine particles i.e., clay and silt (Szymanski, 2021), likely due to loess deposition (Jacobs and Mason, 2007), which enhanced SOM protection. These fine particles, through electrostatic interactions and microaggregate formation (Six et al., 2004), were strong predictors of the radiocarbon age of the slow-cycling SOM pool (Dolui et al., in press). Their influence is further underscored by the superior predictive power of the MLR models for slow-cycling SOM decay rate and pool size, compared to the more transient fast-cycling pool.

Importantly, the slow-cycling SOM pool dominated total soil C (>96%) (Fig. 4b) and increased in size with higher TOC and TIC content (Equation 4) - corresponding with a decline in the fast-cycling pool. The relative size of the fast pool was consistently greater in modern than Brady soils, and in erosional than burial transects, suggesting stronger stabilization in buried paleosols. This highlights the pivotal role of the slow-cycling pool in soil C persistence and its relevance for long-term climate mitigation strategies.

Apparent relationships between sodium adsorption ratio (SAR), exchangeable cation concentrations, decay rates and pool sizes in the MLR models (Equations 4, 5, 6 and 7 and Fig. 6) may be coincidental, reflecting shared depth-dependent trends rather than direct mechanistic links. For instance, studies have typically shown that both TOC and microbial biomass decline with depth (Fierer and Schimel, 2003; Xiang et al., 2008), contributing to reduced respiration in deeper Brady soils. Concurrently, Na tends to accumulate at depth via leaching (Dolui et al., in press) where the depth of accumulation depends on precipitation and soil water status.

4.2 Destabilization of SOM by erosion and moisture variability

The greater cumulative C loss from shallower soils, together with the smaller size of the fast-cycling SOM pool and the significantly lower decay rate of slow-cycling SOM in depositional Brady soils compared to their erosional counterparts (Fig. 4a), underscores the destabilizing effect of surface exposure. Larger CO₂ pulses from the erosional transect during the initial phase of wet–dry cycling (Fig. A1) further support the hypothesis that Brady soils closer to the surface undergo greater mineralization due to priming by root exudates and organic inputs, enhanced by bioturbation (Pausch et al., 2016; McMurtry et al., 2024). This interpretation is consistent with higher fraction modern (radiocarbon abundance) values in erosional versus depositional Brady soils and with the convergence of slow-pool fraction modern in erosional Brady soils toward those of modern soils (Dolui et al., in press).

In the wet-dry experiment, decay patterns further highlighted the role of erosion in destabilization: slow pools decayed faster in erosional than in burial transects, while fast pools decomposed more rapidly in modern than in Brady soils. The fraction of the slow pool was smaller under continuous wetting than under wet-dry cycles, indicating that variable moisture regimes



440

445

450

460

465



promote greater allocation to the slow pool. However, the substantially higher decay rate of the slow pool under wet–dry cycling suggests that this apparent stabilization is temporary and would likely be offset over time by declining reserves of the passive C pool.

Moisture variability also accentuated the behavior of the fast pool. The higher decay rate of the fast pool under wet–dry cycling, especially in modern soils and erosional transects, supports the idea that fresh organic inputs and surface exposure accelerate C turnover under fluctuating moisture. This is reinforced by the MLR model, which revealed a positive correlation between TOC and the fast-cycling SOM decay rate (Equation 7), consistent with stimulation of decomposition by fresh organic inputs. The lack of significant differences in Brady soils, by contrast, suggests that burial dampens moisture-driven variability in labile C turnover.

McDowell et al. (2022) simulated soil hydrology for the Brady Soil and the overlying loess and modern soil, using measured hydraulic properties from the Wauneta site and weather data from 2009-2019. The modeled water content generally remained relatively low and constant in horizons below a depth of 1.5 m, including the Brady Soil, with rare deeper wetting following major rainfall events. The depth of frequent wetting would likely have been even less during the multiple periods of drier-than-modern climate over the past 10,000 yr (Miao et al., 2007). These modeling results and paleo-climatic reconstructions, combined with the effects of moisture on decomposition reported here, suggest that dry conditions have had a major role in sequestration of OC in the the Brady Soil over thousands of years where it is deeply buried, but greater loss could occur with both erosional exposure and a climate that favors more frequent wetting and drying cycles at depth.

5 Conclusion

Our study demonstrates that SOC decomposition is strongly shaped by soil moisture regime and landscape position, with modern and Brady soils responding differently to continuous wetting versus drying–rewetting cycles. Water availability exerted disproportionate effects in erosional settings where surface exposure enhanced substrate diffusivity, highlighting the destabilizing role of re-exposure and moisture fluctuations.

Drying–rewetting cycles led to greater C losses from Brady soils than continuous wetting, despite modeling results indicating dominance of the slow pool and depletion of labile C. This treatment also accelerated fast pool decay in modern soils and erosional transects, while burial dampened such variability in Brady soils. Fraction sizes shifted accordingly: wet–dry cycles increased the proportion of the slow pool and reduced the fast pool fraction, suggesting redistribution of SOC toward more stabilized forms under fluctuating moisture.

Depth further constrained SOM persistence, with slow pool decay constants declining in deeper Brady soils from depositional transects. Faster turnover in shallow layers reflects greater microbial accessibility and responsiveness to surface-driven processes, underscoring the importance of geomorphic context - transect type, burial depth, and soil structure - over intrinsic SOM chemistry.

Comparisons across models showed that continuous wetting accelerated overall decay, particularly in burial transects, while wet–dry cycles disproportionately destabilized the slow pool that dominates SOC. This dual effect - rapid labile C turnover





under moisture fluctuations coupled with erosion of long-lived SOM persistence - points to heightened vulnerability of buried carbon under future precipitation variability.

Overall, the fate of ancient soil carbon under climate change will depend on both its burial history and prevailing moisture regime. Integrating these contrasting controls on fast- and slow-cycling pools into Earth system models is essential for improving predictions of soil carbon vulnerability and climate feedback.

Funding

This work was supported by the National Science Foundation (EAR awards 1623814, 1623810, and 1623812), the University of California, Merced, and the Ted and Jan Falasco Endowment.

475 Competing interests

The authors have no relevant financial or non-financial interests to disclose.

Data availability

Full dataset for soil incubation and statistical analyses are available at DOI: doi: 10.17632/fjw646gpyf.1.

Author contributions

All authors contributed to the study conception and design. Material preparation, data collection, and analysis were performed by Manisha Dolui, Teneille Nel, Abbygail R. McMurtry, Stephanie Chacon, Laura M. Phillips, Teamrat Ghezzehei, Joseph A. Mason, Erika Marin-Spiotta, Marie-Anne de Graaff and Asmeret Asefaw Berhe. The first draft of the manuscript was written by Manisha Dolui and Teneille Nel. All authors commented on previous versions of the manuscript and approved the final manuscript.

485 Acknowledgments

We acknowledge financial support for this work from the National Science Foundation (EAR awards 1623814, 1623810, and 1623812) and the Ted and Jan Falasco Endowment, fellowships and grants awarded by the Graduate Division at the University of California, Merced (UCM), and the UCM Environmental Systems Graduate Group. We are grateful to Dr. Sora Kim and Dr. Robin Trayler for their support at the UCM Stable Isotope Lab. We also thank R. and D. Whiting for providing access to the Wauneta, Nebraska, field sites. ChatGPT was used for language editing and sentence refinement and the authors take full responsibility for the output.





Tables and figures





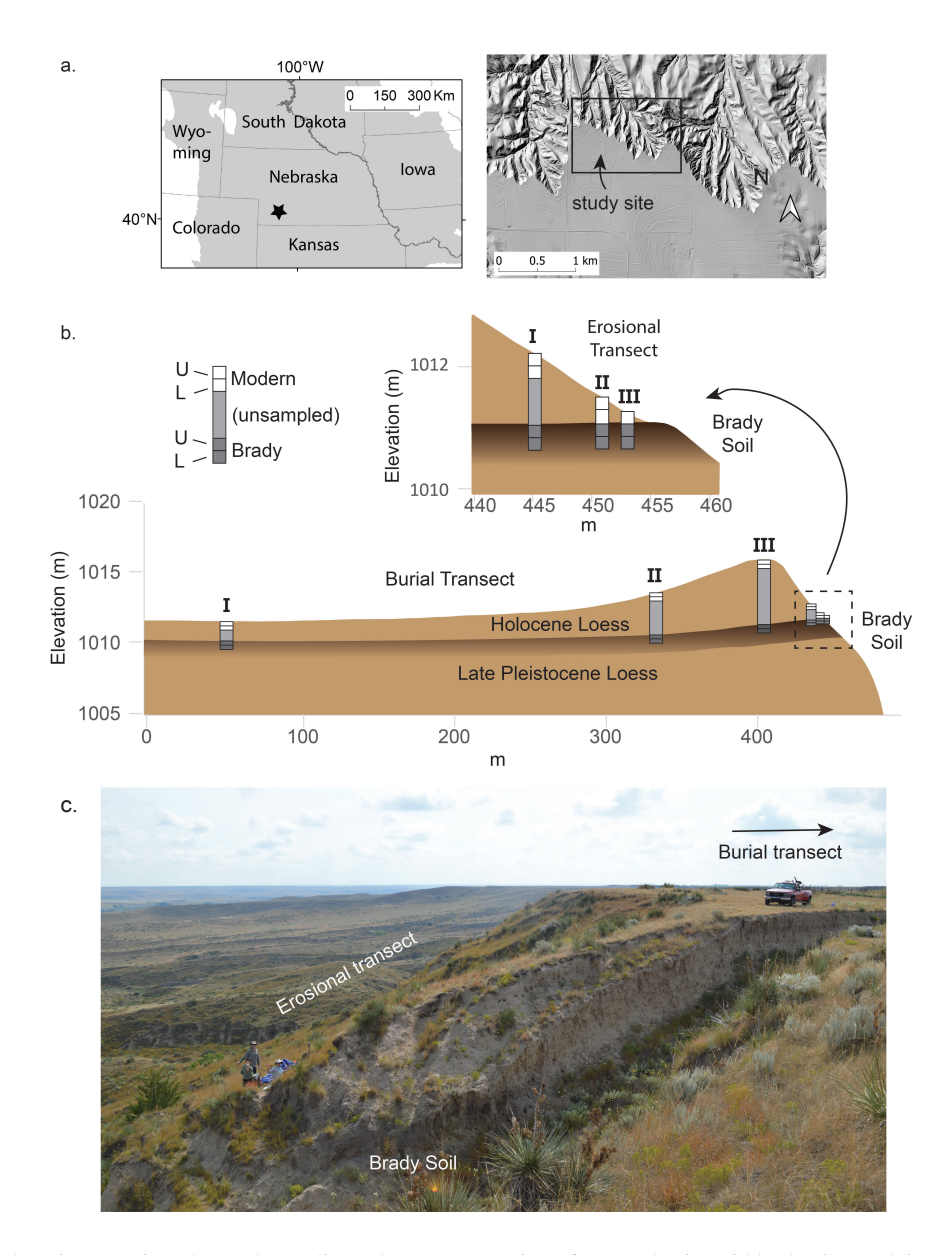


Figure 1. Study site location, stratigraphy, and sampling scheme. a. Location of the study site within the Great Plains ecoregion (grayshade) and shaded relief map illustrating topographic setting of study site.

b. Vertical cross-sections illustrating the sampling scheme relative to modern land surface topography, the Brady Soil, and loess above and below it at study site. Weakly developed horizons of modern soil and paleosols within the Holocene loess (Miao et al., 2007) not shown. Details based on one pair of burial and erosional transects but representative of all three.

c. Photo illustrating topography and native grassland vegetation at one pair of transects. Truck is near deepest profile (III) on burial transect; other burial transect points are not visible. Brady Soil is exposed in an old roadcut in foreground; erosional transect is located on intact slope beyond roadcut. Figure adapted from Dolui et al., in press.





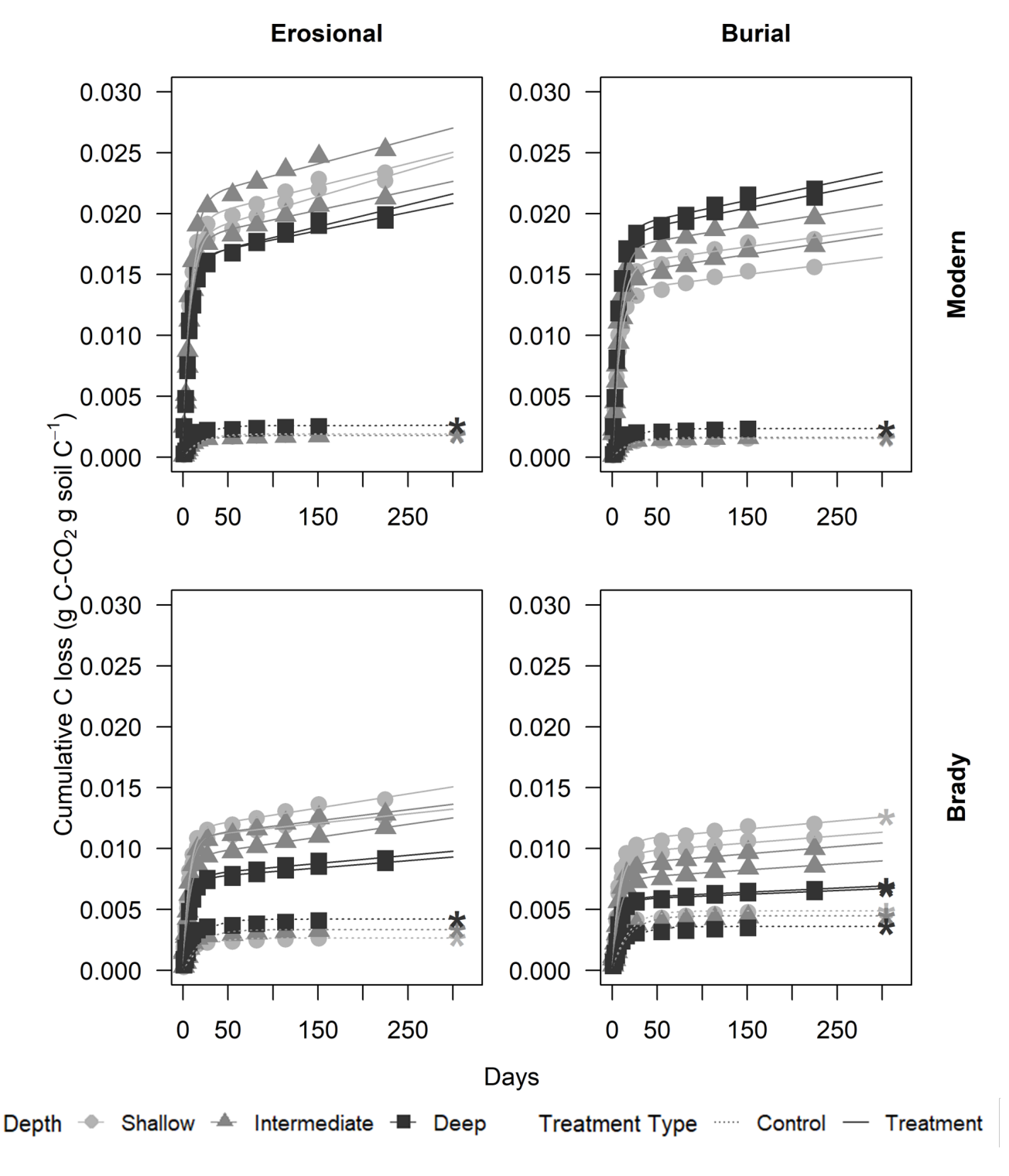


Figure 2. Cumulative respiratory CO₂ from modern and Brady Soil sampled from three depths representing varying degrees of burial/erosional exposure (two technical replicates each). Soils were maintained at a constant moisture content of 60% water holding capacity (WHC). Lines depict a two-pool first-order decay model, fitted using a non-linear least-squares function. The dotted line represents the control (5% WHC).





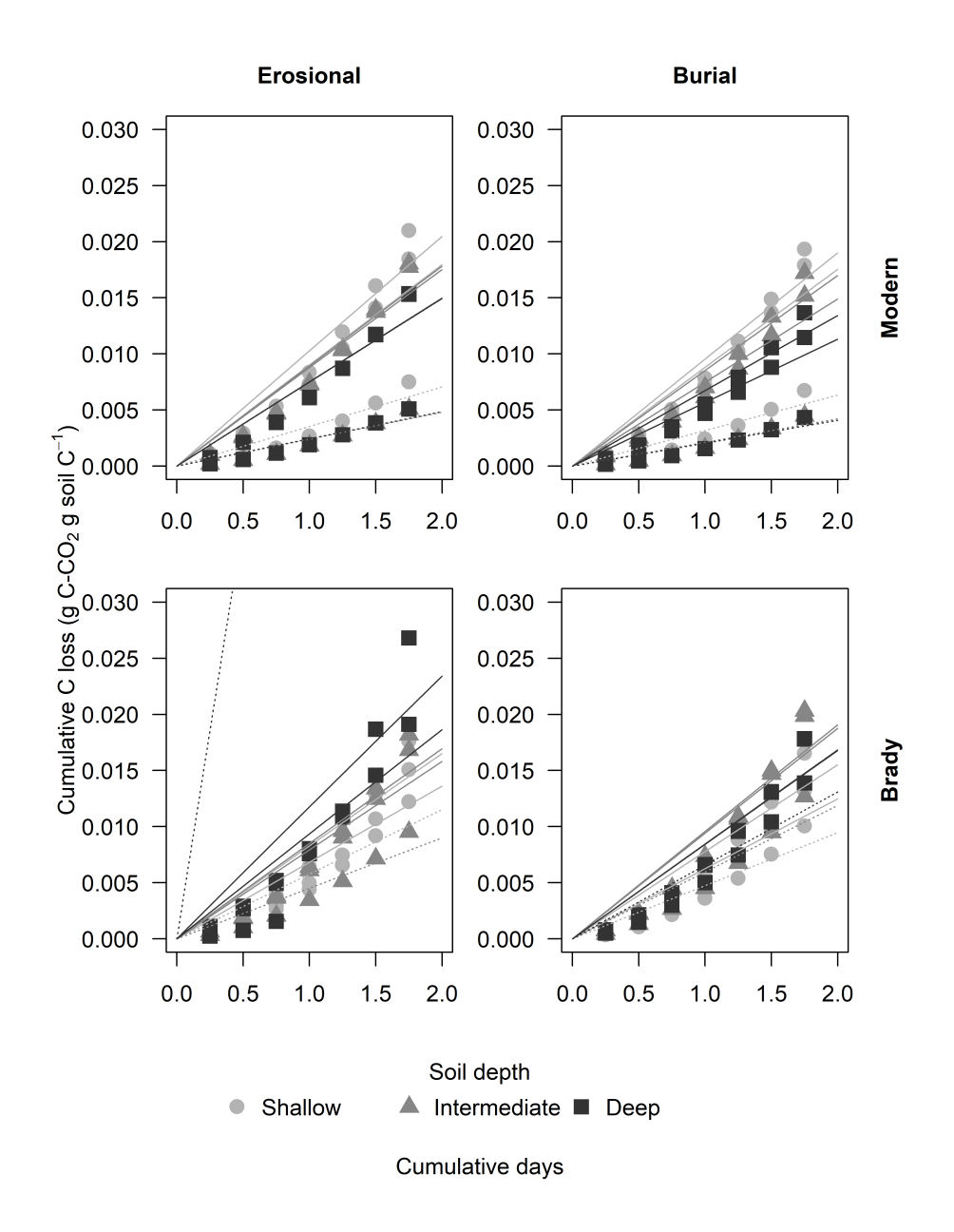


Figure 3. Cumulative respiratory CO₂ flux from modern and Brady Soil sampled from three depths representing varying degrees of burial/erosional exposure (two technical replicates each). Soils were wetted to a moisture content of 60% water holding capacity (WHC) and allowed to dry to 5% WHC. Lines depict a one-pool first-order decay model, fitted using a non-linear least-squares function. The dotted line represents the control (constant 5% WHC); one control Brady soil sample of the erosional transect had an outlier point not shown due to scale.





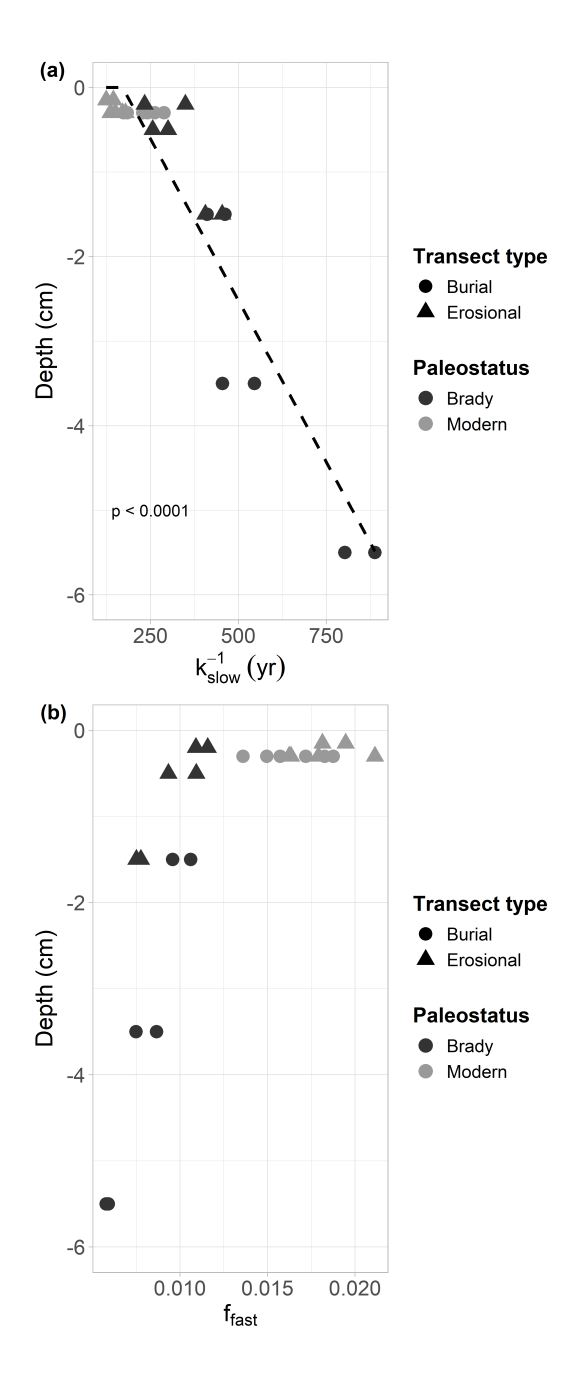


Figure 4. Decay constant of the slow cycling pool of modern and Brady soils incubated under continuously wet conditions. Samples collected from depositional and erosional transect types. Dotted line indicates exponential decay. Figure b indicates the size of the fast-cycling pool at different depths of the modern and Brady soils in depositional and erosional transect types.





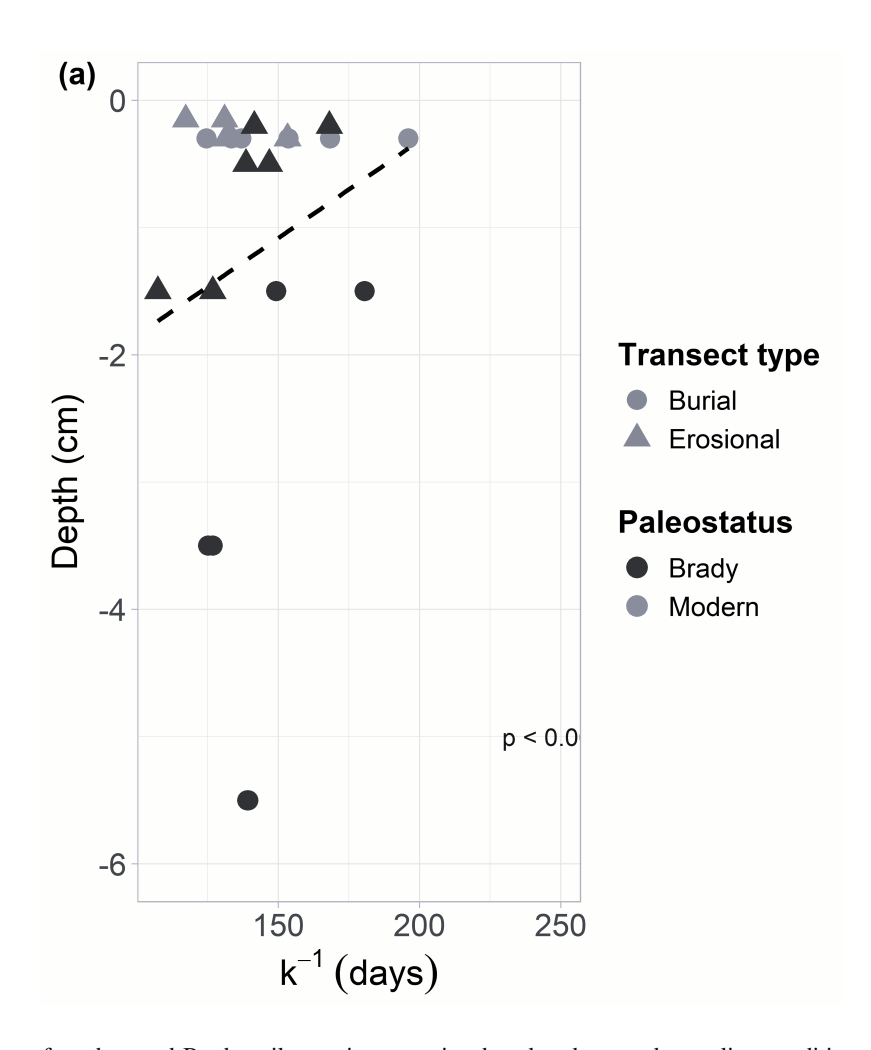


Figure 5. Decay constant of modern and Brady soil organic matter incubated under wet-dry cycling conditions. Samples collected from depositional and erosional transect types. Dotted line indicates exponential decay.





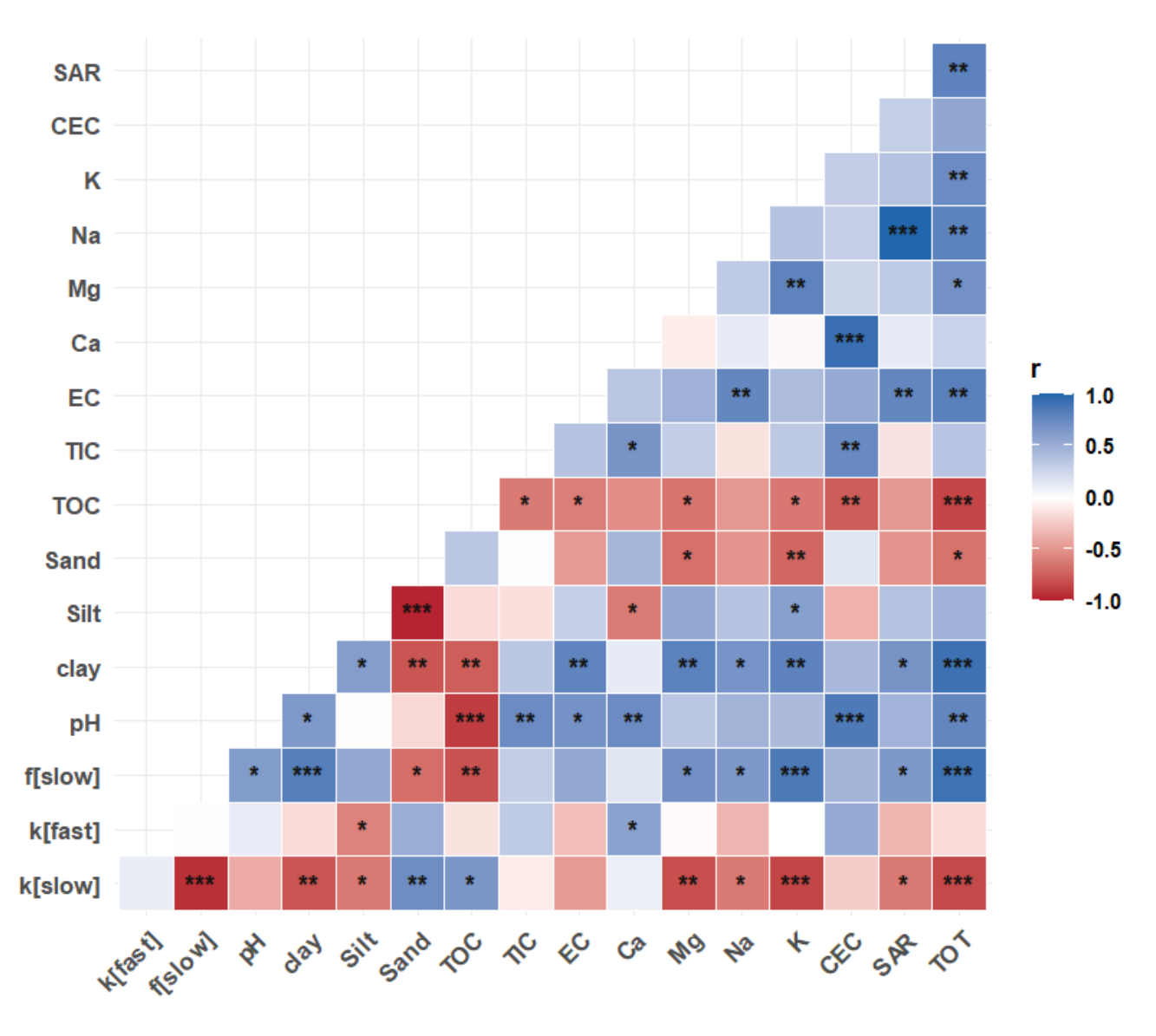


Figure 6. Correlation between soil physicochemical properties and modeled soil organic matter decomposition parameters (decay constant, k, and fraction of C in slow pool, f) for fast- and slow-cycling pools in modern and Brady soils incubated under continuously wet conditions. Decomposition parameters were obtained by multiple linear regression across burial and erosional transects. The statistical significance of each correlation is denoted by asterisks (*** for p<0.001, ** for p<0.01, * for p<0.05).





Table 1. General physicochemical (mean \pm standard deviation) of soils used in the incubation experiment, grouped by transect type and paleostatus

Transect type	Bur	rial	Eros	ional
Paleostatus	Brady	Modern	Brady	Modern
pH	7.77 ± 0.04	6.89 ± 0.32	7.68 ± 0.12	7.41 ± 0.10
Clay (%)	9.48 ± 0.75	6.13 ± 0.64	7.62 ± 0.44	6.29 ± 0.48
Silt (%)	59.31 ± 0.44	56.24 ± 5.76	55.73 ± 4.88	53.67 ± 1.51
Sand (%)	31.24 ± 0.94	37.62 ± 6.39	36.64 ± 5.22	40.08 ± 1.92
TOC content	0.45 ± 0.06	1.03 ± 0.20	0.56 ± 0.10	0.93 ± 0.17
TIC content	0.24 ± 0.11	0.09 ± 0.03	0.28 ± 0.04	0.25 ± 0.03
$EC (dS m^{-1})$	5.41 ± 0.32	2.26 ± 0.43	3.05 ± 0.47	3.57 ± 0.35
${\rm CEC}\;({\rm cmolckg}^{-1})$	22.86 ± 0.54	15.17 ± 3.54	23.31 ± 3.52	20.59 ± 1.83
Turnover time (y)	15654 ± 2440	576.4 ± 126	8327 ± 2732	1451 ± 673
CN ratio	10.00 ± 0.45	9.24 ± 0.21	10.96 ± 0.20	9.76 ± 0.25





Table 2. Soil organic matter (SOM) decomposition parameters (decay rate k of one-pool model, decay rates of fast- (k_{fast}) and slow-cycling (k_{slow}) SOM pools, and fraction sizes of fast (f_{fast}) and slow (f_{slow}) pools, grouped by experiment, transect type, and paleostatus.

Experiment		C	W			W	'D	
Transect type	Bu	rial	Eros	ional	Ви	ırial	Eros	sional
Paleostatus	Brady	Modern	Brady	Modern	Brady	Modern	Brady	Modern
k (one pool)	0.0107	0.0099	0.0069	0.0072	0.0071	0.0067	0.0074	0.0074
$k_{ m slow}$	< 0.0001	< 0.0001	< 0.0001	< 0.0001	0.0080	0.0074	0.0086	0.0084
$k_{ m fast}$	0.1250	0.1264	0.1333	0.1270	0.6931	6.3419	0.4222	9.8728
$f_{ m slow}$	0.9920	0.9836	0.9903	0.9818	0.9990	0.9990	0.9990	0.9990
$f_{ m fast}$	0.0080	0.0164	0.0097	0.0182	0.0010	0.0010	0.0010	0.0010





Appendix A: Sampling Depth Information





Table A1. Sampling depth intervals (standard deviation in brackets for n = 3) of modern (surface) and Brady (burial) soils along two types of transects, where degrees of burial or exposure increase from degrees I to III. Table adapted from Dolui et al., in press.

				Trans	Transect Type		
			Erosional			Burial	
				ď	Degree		
	Depth (cm) III	Ш	Π	I	I	П	Ш
	M. J	0-19 (2.5)	0-19 (2.5) 0-19 (3.2) 0-18 (3.5)	0-18 (3.5)	0-30 (0.6)	0-29 (0.6)	0-29 (0.0)
D. 1.0.404	Modelli	NA	19-38 (3.6)	19-38 (3.6) 18-36 (3.5)	30-60 (0.6)	29-59 (2.3)	29-59 (2.3)
raieostatus		20-50 (1.2)	50-80 (0.0)	150-180 (0.0)	100-130 (4.0)	20-50 (1.2) 50-80 (0.0) 150-180 (0.0) 100-130 (4.0) 300-330 (9.3) 550-580 (6.7)	550-580 (6.7)
	brauy	50-80 (0.4)	80-120 (0.0)	180-210 (2.9)	130-160 (4.5)	50-80 (0.4) 80-120 (0.0) 180-210 (2.9) 130-160 (4.5) 330-360 (2.6) 580-610 (5.6)	580-610 (5.6)





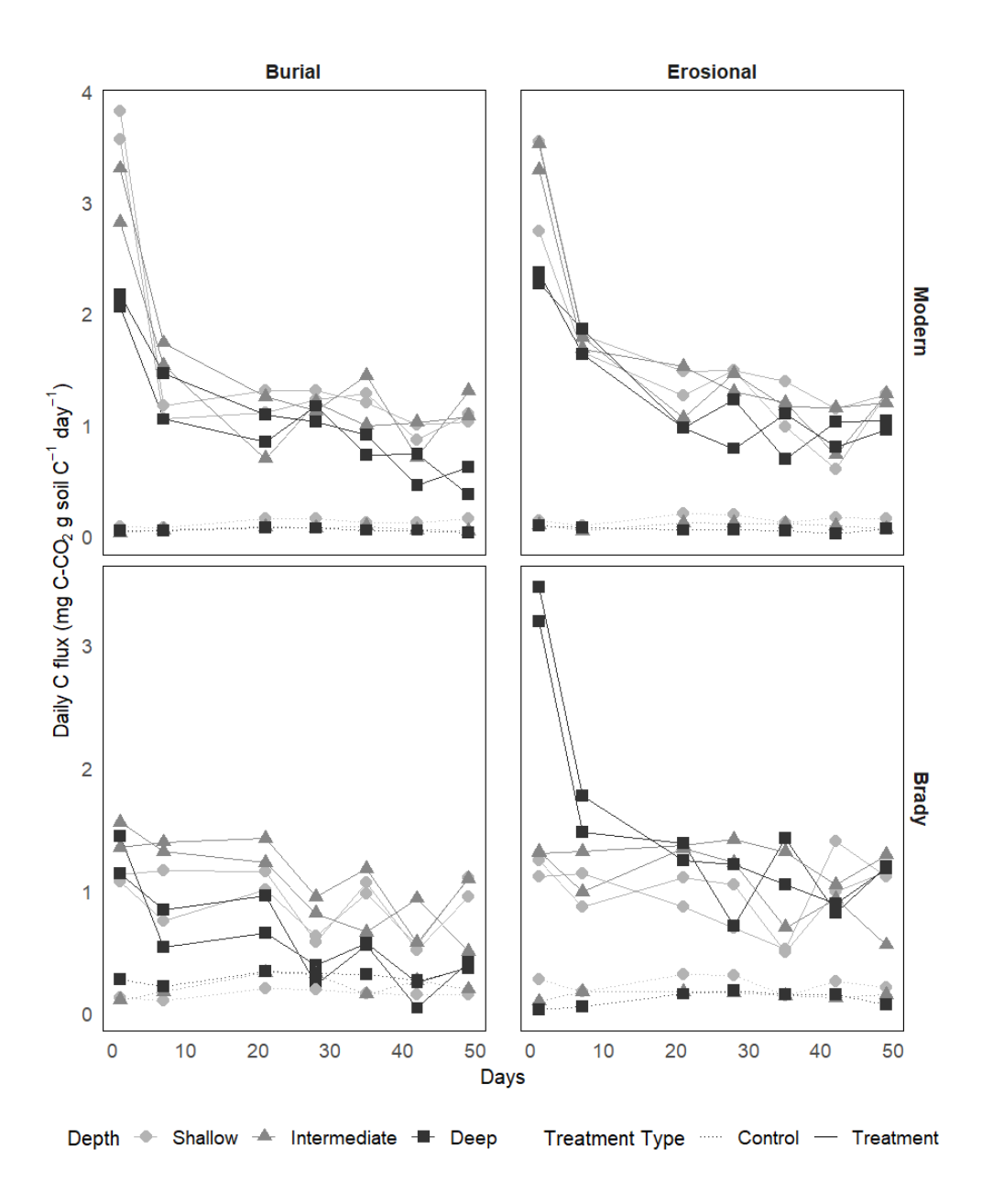


Figure A1. Daily respiratory CO_2 flux from modern and Brady Soil sampled from three depths representing varying degrees of burial/erosional exposure (two technical replicates each). Soils were wetted to a moisture content of 60% water holding capacity (WHC) and allowed to dry to 5% WHC. The dotted line represents the control (constant 5% WHC).





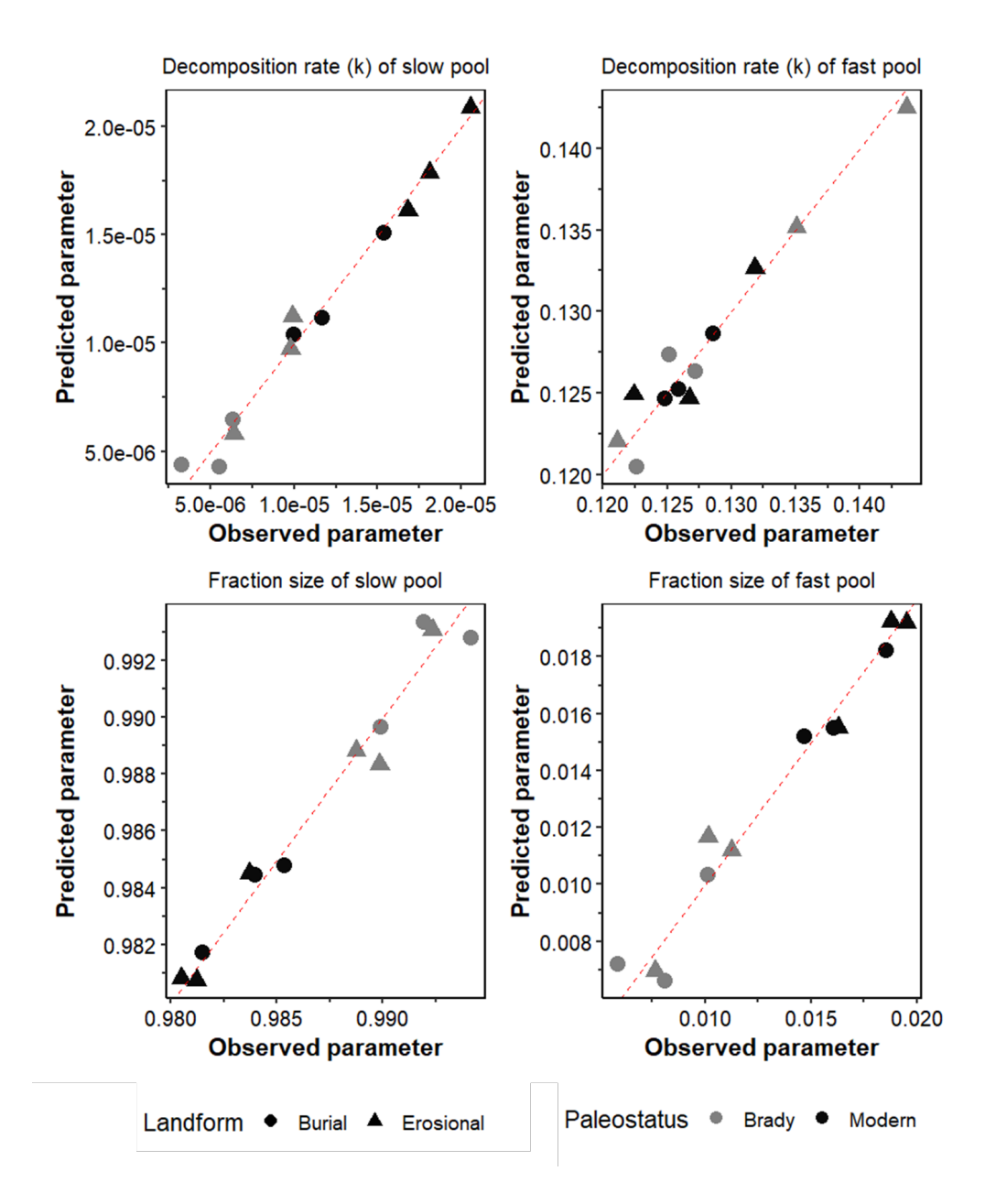


Figure A2. True versus predicted soil organic matter decomposition parameters (decay constant, k, and fraction of C in slow pool, f) for fast-and slow-cycling pools in modern and Brady soils incubated under continuously wet conditions. These parameters were obtained by multiple linear regression across burial and erosional transects. Red dotted line represents y = x.





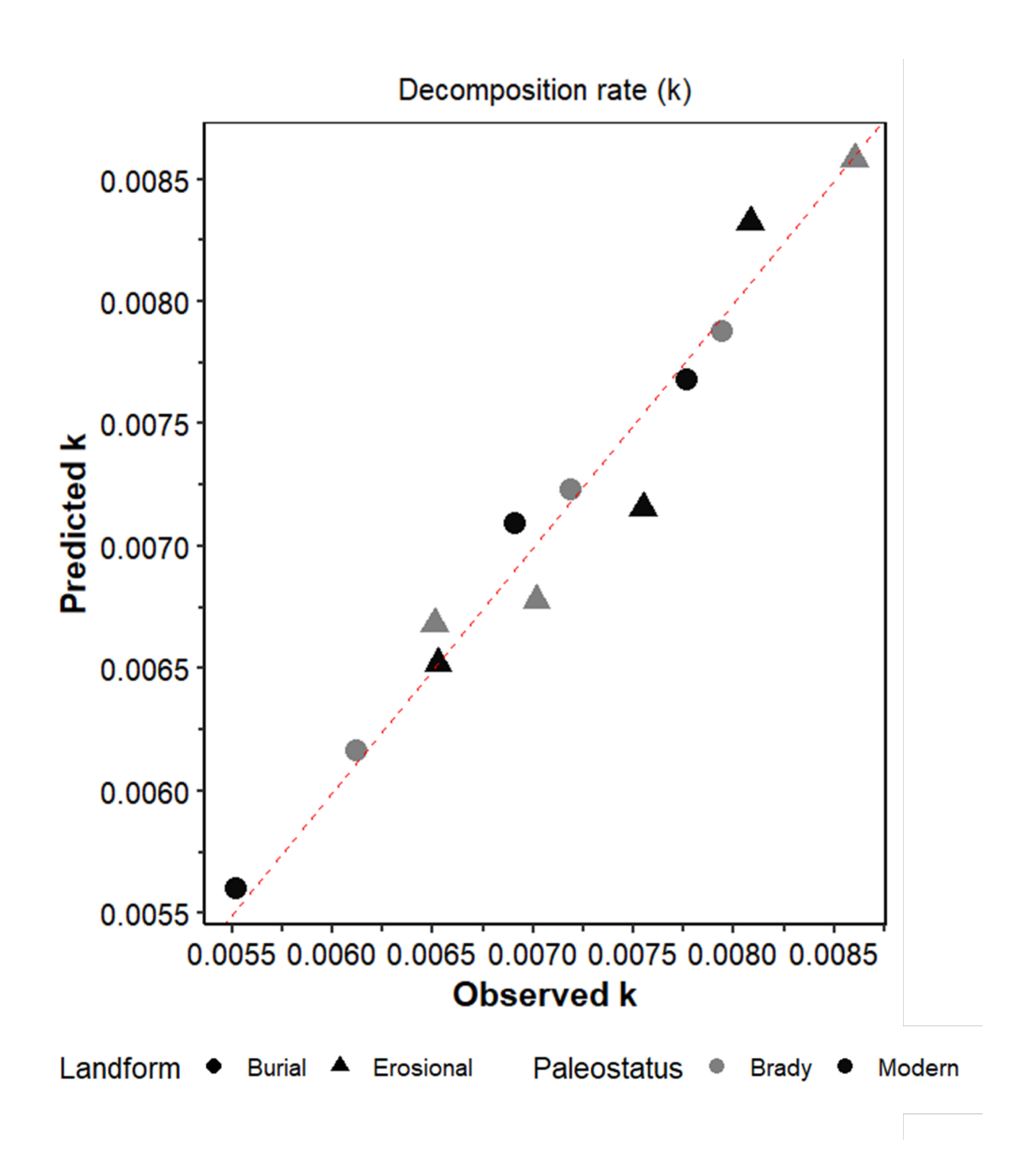


Figure A3. True versus predicted soil organic matter decay constant, k) in modern and Brady soils incubated under wet-dry cycling conditions. These parameters were obtained by multiple linear regression across burial and erosional transects. Red dotted line represents y = x.





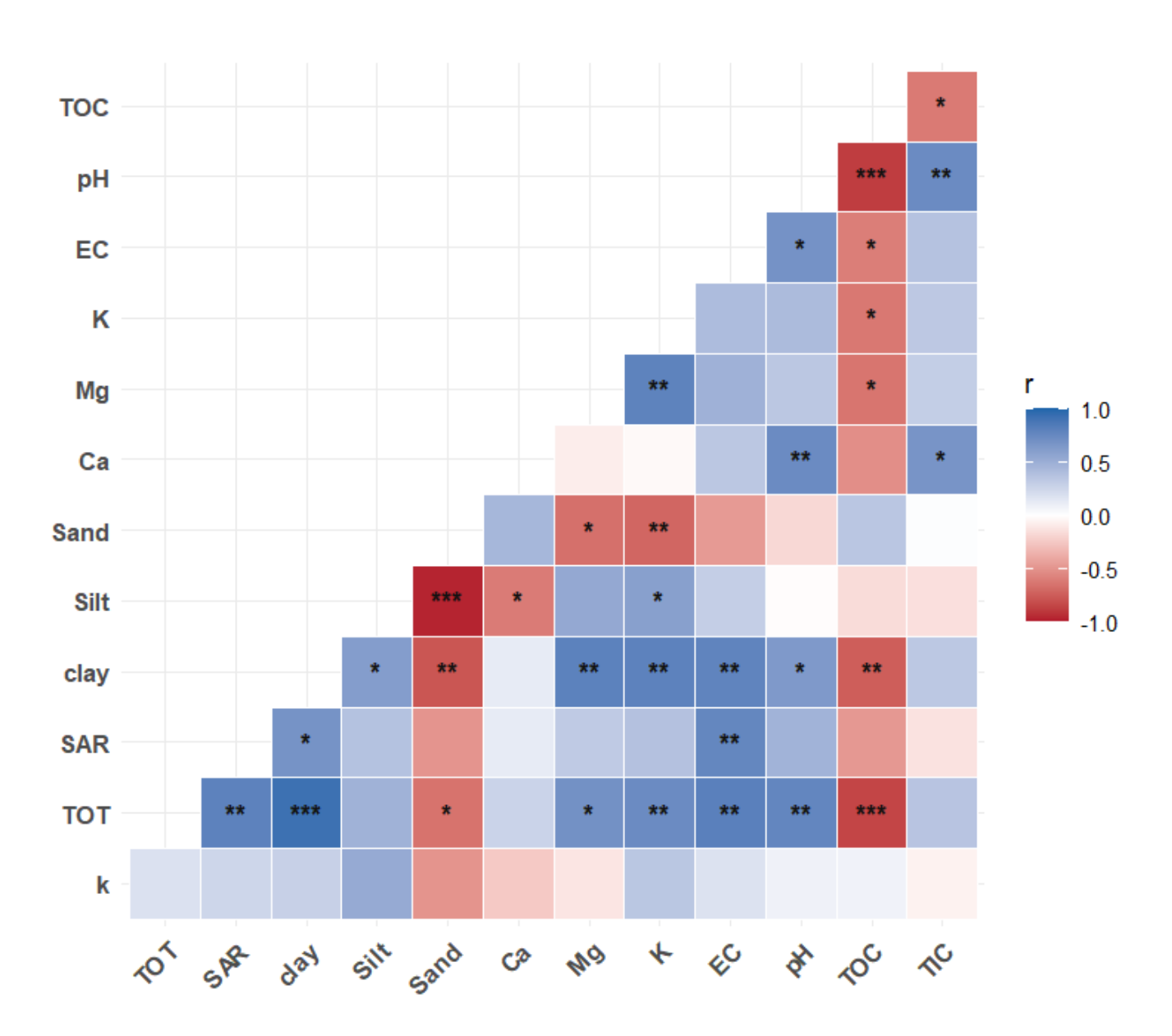


Figure A4. Correlation between soil physicochemical properties and modeled soil organic matter decomposition parameters (decay constant, k, and fraction of C in slow pool, f) for fast- and slow-cycling pools in modern and Brady soils incubated under wet-dry cycles. Decomposition parameters were obtained by multiple linear regression across burial and erosional transects. The statistical significance of each correlation is denoted by asterisks (*** for p < 0.001, ** for p < 0.01, * for p < 0.05).





References

505

- Batool, M., Cihacek, L. J., and Alghamdi, R. S.: Soil Inorganic Carbon Formation and the Sequestration of Secondary Carbonates in Global Carbon Pools: A Review, Soil Systems, 8, 15, https://doi.org/10.3390/soilsystems8010015, 2024.
 - Beare, M., Gregorich, E., and St-Georges, P.: Compaction effects on CO2 and N2O production during drying and rewetting of soil, Soil Biology and Biochemistry, 41, 611–621, https://doi.org/10.1016/j.soilbio.2008.12.024, 2009.
- Berhe, A. A., Harte, J., Harden, J. W., and Torn, M. S.: The Significance of the Erosion-induced Terrestrial Carbon Sink, BioScience, 57, 337–346, https://doi.org/10.1641/B570408, 2007.
 - Berhe, A. A., Harden, J. W., Torn, M. S., and Harte, J.: Linking soil organic matter dynamics and erosion-induced terrestrial carbon sequestration at different landform positions, Journal of Geophysical Research: Biogeosciences, 113, https://doi.org/10.1029/2008JG000751, 2008.
 - Berhe, A. A., Suttle, K. B., Burton, S. D., and Banfield, J. F.: Contingency in the direction and mechanics of soil organic matter responses to increased rainfall, Plant and Soil, 358, 371–383, https://doi.org/10.1007/s11104-012-1156-0, 2012.
 - Berhe, A. A., Barnes, R. T., Six, J., and Marín-Spiotta, E.: Role of Soil Erosion in Biogeochemical Cycling of Essential Elements: Carbon, Nitrogen, and Phosphorus, Annual Review of Earth and Planetary Sciences, 46, 521–548, https://doi.org/10.1146/annurev-earth-082517-010018, 2018.
- Bird, J. A. and Torn, M. S.: Fine Roots vs. Needles: A Comparison of 13C and 15N Dynamics in a Ponderosa Pine Forest Soil, Biogeochemistry, 79, 361–382, https://doi.org/10.1007/s10533-005-5632-y, 2006.
 - Chaopricha, N. T.: The Importance, Origin, Composition, and Stability of Deeply Buried Soil Organic Matter, Ph.D. thesis, University of Wisconsin-Madison, Madison, 2013.
 - Chaopricha, N. T. and Marín-Spiotta, E.: Soil burial contributes to deep soil organic carbon storage, Soil Biology and Biochemistry, 69, 251–264, https://doi.org/10.1016/j.soilbio.2013.11.011, 2014.
- Chowdhury, N., Marschner, P., and Burns, R. G.: Soil microbial activity and community composition: Impact of changes in matric and osmotic potential, Soil Biology and Biochemistry, 43, 1229–1236, https://doi.org/10.1016/j.soilbio.2011.02.012, 2011.
 - Cotrufo, M. F. and Lavallee, J. M.: Incorporating aridity in soil carbon stewardship frameworks, Nature Climate Change, 15, 240–242, https://doi.org/10.1038/s41558-025-02270-9, 2025.
- Davidson, E. A., Samanta, S., Caramori, S. S., and Savage, K.: The <scp>D</scp> ual <scp>A</scp> rrhenius and <scp>M</scp> ichaelis— <scp>M</scp> enten kinetics model for decomposition of soil organic matter at hourly to seasonal time scales, Global Change Biology, 18, 371–384, https://doi.org/10.1111/j.1365-2486.2011.02546.x, 2012.
 - Elzhov, T., Mullen, K., Spiess, A., and Bolker, B.: minpack.lm: R Interface to the Levenberg-Marquardt Nonlinear Least-Squares Algorithm Found in MINPACK, Plus Support for Bounds., https://CRAN.R-project.org/package=minpack.lm., 2023.
- Fierer, N. and Schimel, J. P.: A Proposed Mechanism for the Pulse in Carbon Dioxide Production Commonly Observed Following the Rapid
 Rewetting of a Dry Soil, Soil Science Society of America Journal, 67, 798, https://doi.org/10.2136/sssaj2003.0798, 2003.
 - Fontaine, S., Barré, P., Bdioui, N., Mary, B., and Rumpel, C.: Stability of organic carbon in deep soil layers controlled by fresh carbon supply, Nature, 450, 277–280, https://doi.org/10.1038/nature06275, 2007.
 - Gao, X., Huang, R., Li, J., Wang, C., Lan, T., Li, Q., Deng, O., Tao, Q., and Zeng, M.: Temperature induces soil organic carbon mineralization in urban park green spaces, Chengdu, southwestern China: Effects of planting years and vegetation types, Urban Forestry & Urban Greening, 54, 126761, https://doi.org/10.1016/j.ufug.2020.126761, 2020.





- Ghezzehei, T. A., Sulman, B., Arnold, C. L., Bogie, N. A., and Berhe, A. A.: On the role of soil water retention characteristic on aerobic microbial respiration, Biogeosciences, 16, 1187–1209, https://doi.org/10.5194/bg-16-1187-2019, 2019.
- Goebel, M.-O., Bachmann, J., Woche, S. K., and Fischer, W. R.: Soil wettability, aggregate stability, and the decomposition of soil organic matter, Geoderma, 128, 80–93, https://doi.org/10.1016/j.geoderma.2004.12.016, 2005.
- Griffiths, B. S. and Philippot, L.: Insights into the resistance and resilience of the soil microbial community, FEMS Microbiology Reviews, 37, 112–129, https://doi.org/10.1111/j.1574-6976.2012.00343.x, 2013.
 - Hicks Pries, C. E., Castanha, C., Porras, R. C., and Torn, M. S.: The whole-soil carbon flux in response to warming, Science, 355, 1420–1423, https://doi.org/10.1126/science.aal1319, 2017.
- Hicks Pries, C. E., Ryals, R., Zhu, B., Min, K., Cooper, A., Goldsmith, S., Pett-Ridge, J., Torn, M., and Berhe, A. A.: The
 Deep Soil Organic Carbon Response to Global Change, Annual Review of Ecology, Evolution, and Systematics, 54, 375–401, https://doi.org/10.1146/annurev-ecolsys-102320-085332, 2023.
 - Hill, R. L., Horton, R., and Cruse, R. M.: Tillage Effects on Soil Water Retention and Pore Size Distribution of Two Mollisols, Soil Science Society of America Journal, 49, 1264–1270, https://doi.org/10.2136/sssai1985.03615995004900050039x, 1985.
- Horne, D. and McIntosh, J.: Hydrophobic compounds in sands in New Zealand—extraction, characterisation and proposed mechanisms for repellency expression, Journal of Hydrology, 231-232, 35–46, https://doi.org/10.1016/S0022-1694(00)00181-5, 2000.
 - IPCC: Global Warming of 1.5°C., in: An IPCC Special Report on the impacts of global warming of 1.5°C above pre-industrial levels and related global greenhouse gas emission pathways, in the context of strengthening the global response to the threat of climate change, edited by Masson-Delmotte, V., Zhai, P., Pörtner, H.-O., Roberts, D., Skea, J., Shukla, P., Pirani, A., Moufouma-Okia, W., Péan, C., Pidcock, R., Connors, S., Matthews, J., Chen, Y., Zhou, X., Gomis, M., Lonnoy, E., Maycock, T., Tignor, M., and Waterfield, T., Intergovernmental Panel on Climate Change., https://doi.org/10.1038/291285a0, 2018.
 - Jacobs, P. M. and Mason, J. A.: Paleopedology of soils in thick Holocene loess, Nebraska, USA, Revista Mexicana de Ciencias Geológicas, 21, 54–70, 2004.
 - Jacobs, P. M. and Mason, J. A.: Late Quaternary climate change, loess sedimentation, and soil profile development in the central Great Plains: A pedosedimentary model, Geological Society of America Bulletin, 119, 462–475, https://doi.org/10.1130/B25868.1, 2007.
- Jobbagy, E. G. and Jackson, R. B.: The Vertical Distribution of Soil Organic Carbon and Its Relation to Climate and Vegetation, Ecological Applications, 10, 423–436, 2000.
 - Johnson, W. C. and Willey, K. L.: Isotopic and rock magnetic expression of environmental change at the Pleistocene–Holocene transition in the central Great Plains, Quaternary International, 67, 89–106, https://doi.org/10.1016/S1040-6182(00)00011-2, 2000.
- Johnson, W. C., Willey, K. L., Mason, J. A., and May, D. W.: Stratigraphy and environmental reconstruction at the middle Wisconsinan Gilman Canyon formation type locality, Buzzard's Roost, southwestern Nebraska, USA, Quaternary Research, 67, 474–486, https://doi.org/10.1016/j.yqres.2007.01.011, 2007.
 - Kaiser, M., Kleber, M., and Berhe, A. A.: How air-drying and rewetting modify soil organic matter characteristics: An assessment to improve data interpretation and inference, Soil Biology and Biochemistry, 80, 324–340, https://doi.org/10.1016/j.soilbio.2014.10.018, 2015.
- Kang, S. and Xing, B.: Humic Acid Fractionation upon Sequential Adsorption onto Goethite, Langmuir, 24, 2525–2531, https://doi.org/10.1021/la702914q, 2008.
 - Kemper, W. D., Rosenau, R. C., and Dexter, A. R.: Cohesion Development in Disrupted Soils as Affected by Clay and Organic Matter Content and Temperature, Soil Science Society of America Journal, 51, 860–867, https://doi.org/10.2136/sssaj1987.03615995005100040004x, 1987.





- Leizeaga, A., Hicks, L. C., Manoharan, L., Hawkes, C. V., and Rousk, J.: Drought legacy affects microbial community trait distributions related to moisture along a savannah grassland precipitation gradient, Journal of Ecology, 109, 3195–3210, https://doi.org/10.1111/1365-2745.13550, 2021.
 - Lenth, R. V.: emmeans: Estimated Marginal Means, aka Least-Squares Means, https://CRAN.R-project.org/package=emmeans, 2024.
 - Li, Q., Hu, W., Li, L., and Li, Y.: Interactions between organic matter and Fe oxides at soil micro-interfaces: Quantification, associations, and influencing factors, Science of The Total Environment, 855, 158 710, https://doi.org/10.1016/j.scitotenv.2022.158710, 2023.
- Liu, T., Wang, L., Feng, X., Zhang, J., Ma, T., Wang, X., and Liu, Z.: Comparing soil carbon loss through respiration and leaching under extreme precipitation events in arid and semiarid grasslands, Biogeosciences, 15, 1627–1641, https://doi.org/10.5194/bg-15-1627-2018, 2018.
 - Marin-Spiotta, E., Chadwick, O. A., Kramer, M., and Carbone, M. S.: Carbon delivery to deep mineral horizons in Hawaiian rain forest soils, Journal of Geophysical Research, 116, G03 011, https://doi.org/10.1029/2010JG001587, 2011.
- Marin-Spiotta, E., Chaopricha, N. T., Plante, A. F., Diefendorf, A. F., Mueller, C. W., Grandy, A. S., and Mason, J. A.: Long-term stabilization of deep soil carbon by fire and burial during early Holocene climate change, Nature Geoscience, 7, 428–432, https://doi.org/10.1038/ngeo2169, 2014.
 - Mason, J. A., Jacobs, P. M., Hanson, P. R., Miao, X., and Goble, R. J.: Sources and paleoclimatic significance of Holocene Bignell Loess, central Great Plains, USA, Quaternary Research, 60, 330–339, https://doi.org/10.1016/j.yqres.2003.07.005, 2003.
- Mason, J. A., Miao, X., Hanson, P. R., Johnson, W. C., Jacobs, P. M., and Goble, R. J.: Loess record of the Pleistocene–Holocene transition on the northern and central Great Plains, USA, Quaternary Science Reviews, 27, 1772–1783, https://doi.org/10.1016/j.quascirev.2008.07.004, 2008.
 - McDowell, T.: Processes controlling soil hydrology and pedogenic carbonate formation in loess tablelands, Nebraska, USA, Ph.D. thesis, University of Wisconsin-Madison, Madison, 2020.
- 590 McDowell, T. M., Mason, J. A., Vo, T., and Marin-Spiotta, E.: Hydrology of a Semiarid Loess-Paleosol Sequence, and Implications for Buried Soil Connection to the Modern Climate, Plant-Available Moisture, and Loess Tableland Persistence, Journal of Geophysical Research: Earth Surface, 127, https://doi.org/10.1029/2022JF006800, 2022.
- McMurtry, A. R., Kasmerchak, C. S., Vaughan, E. A., Dolui, M., Phillips, L. M., Mueller, C. W., Pett-Ridge, J., Berhe, A. A., Mason, J. A., Marín-Spiotta, E., and de Graaff, M.-A.: Getting to the root of the problem: Soil carbon and microbial responses to root inputs within a buried paleosol along an eroding hillslope in southwestern Nebraska, USA, Soil Biology and Biochemistry, 198, 109 549, https://doi.org/10.1016/j.soilbio.2024.109549, 2024.
 - Miao, X., Mason, J. A., Swinehart, J. B., Loope, D. B., Hanson, P. R., Goble, R. J., and Liu, X.: A 10,000 year record of dune activity, dust storms, and severe drought in the central Great Plains, Geology, 35, 119, https://doi.org/10.1130/G23133A.1, 2007.
 - Miller, A., Schimel, J., Meixner, T., Sickman, J., and Melack, J.: Episodic rewetting enhances carbon and nitrogen release from chaparral soils, Soil Biology and Biochemistry, 37, 2195–2204, https://doi.org/10.1016/j.soilbio.2005.03.021, 2005.
 - Min, K., Berhe, A. A., Khoi, C. M., van Asperen, H., Gillabel, J., and Six, J.: Differential effects of wetting and drying on soil CO2 concentration and flux in near-surface vs. deep soil layers, Biogeochemistry, 148, 255–269, https://doi.org/10.1007/s10533-020-00658-7, 2020
- Najera, F., Dippold, M. A., Boy, J., Seguel, O., Koester, M., Stock, S., Merino, C., Kuzyakov, Y., and Matus, F.: Effects of dry-ing/rewetting on soil aggregate dynamics and implications for organic matter turnover, Biology and Fertility of Soils, 56, 893–905, https://doi.org/10.1007/s00374-020-01469-6, 2020.





- Naorem, A., Jayaraman, S., Dalal, R. C., Patra, A., Rao, C. S., and Lal, R.: Soil Inorganic Carbon as a Potential Sink in Carbon Storage in Dryland Soils—A Review, Agriculture, 12, 1256, https://doi.org/10.3390/agriculture12081256, 2022.
- Neff, J. C. and Asner, G. P.: Dissolved Organic Carbon in Terrestrial Ecosystems: Synthesis and a Model, Ecosystems, 4, 29–48, https://doi.org/10.1007/s100210000058, 2001.
 - Or, D. and Tuller, M.: Liquid retention and interfacial area in variably saturated porous media: Upscaling from single-pore to sample-scale model, Water Resources Research, 35, 3591–3605, https://doi.org/10.1029/1999WR900262, 1999.
 - Pal, S. C., Chakrabortty, R., Towfiqul Islam, A. R. M., Roy, P., Chowdhuri, I., Saha, A., Islam, A., Costache, R., and Alam, E.: Land use and climate change-induced soil erosion mapping in a sub-tropical environment, Geomatics, Natural Hazards and Risk, 14, https://doi.org/10.1080/19475705.2023.2270129, 2023.
 - Pausch, J., Loeppmann, S., Kühnel, A., Forbush, K., Kuzyakov, Y., and Cheng, W.: Rhizosphere priming of barley with and without root hairs, Soil Biology and Biochemistry, 100, 74–82, https://doi.org/10.1016/j.soilbio.2016.05.009, 2016.
 - Pinheiro, J., Bates, D., DebRoy, S., Sarkar, D., and R Core Team: nlme: Linear and Nonlinear Mixed Effects Models, https://CRAN.R-project.org/package=nlme, 2024.
- 620 R Core Team: R: A Language and Environment for Statistical Computing, https://www.r-project.org/, 2025.
 - RStudio Team: RStudio: Integrated Development for R. RStudio, http://www.rstudio.com/, 2019.
 - Rumpel, C. and Kögel-Knabner, I.: Deep soil organic matter—a key but poorly understood component of terrestrial C cycle, Plant and Soil, 338, 143–158, https://doi.org/10.1007/s11104-010-0391-5, 2011.
- Schmidt, M. W. I., Torn, M. S., Abiven, S., Dittmar, T., Guggenberger, G., Janssens, I. A., Kleber, M., Kögel-Knabner, I., Lehmann, J.,
 Manning, D. A. C., Nannipieri, P., Rasse, D. P., Weiner, S., and Trumbore, S. E.: Persistence of soil organic matter as an ecosystem property, Nature, 478, 49–56, https://doi.org/10.1038/nature10386, 2011.
 - Schrumpf, M., Kaiser, K., Guggenberger, G., Persson, T., Kögel-Knabner, I., and Schulze, E.-D.: Storage and stability of organic carbon in soils as related to depth, occlusion within aggregates, and attachment to minerals, Biogeosciences, 10, 1675–1691, https://doi.org/10.5194/bg-10-1675-2013, 2013.
- Sharififar, A., Minasny, B., Arrouays, D., Boulonne, L., Chevallier, T., van Deventer, P., Field, D. J., Gomez, C., Jang, H.-J., Jeon, S.-H., Koch, J., McBratney, A. B., Malone, B. P., Marchant, B. P., Martin, M. P., Monger, C., Munera-Echeverri, J.-L., Padarian, J., Pfeiffer, M., Richer-de Forges, A. C., Saby, N. P., Singh, K., Song, X.-D., Zamanian, K., Zhang, G.-L., and van Zijl, G.: Soil inorganic carbon, the other and equally important soil carbon pool: Distribution, controlling factors, and the impact of climate change, pp. 165–231, https://doi.org/10.1016/bs.agron.2022.11.005, 2023.
- 635 Six, J., Bossuyt, H., Degryze, S., and Denef, K.: A history of research on the link between (micro)aggregates, soil biota, and soil organic matter dynamics, Soil and Tillage Research, 79, 7–31, https://doi.org/10.1016/j.still.2004.03.008, 2004.
 - Soong, J. L., Castanha, C., Hicks Pries, C. E., Ofiti, N., Porras, R. C., Riley, W. J., Schmidt, M. W., and Torn, M. S.: Five years of whole-soil warming led to loss of subsoil carbon stocks and increased CO ₂ efflux, Science Advances, 7, https://doi.org/10.1126/sciadv.abd1343, 2021.
- Stacy, E. M., Hart, S. C., Hunsaker, C. T., Johnson, D. W., and Berhe, A. A.: Soil carbon and nitrogen erosion in forested catchments: implications for erosion-induced terrestrial carbon sequestration, Biogeosciences, 12, 4861–4874, https://doi.org/10.5194/bg-12-4861-2015, 2015.





- Steenwerth, K., Jackson, L., Calderon, F., Scow, K., and Rolston, D.: Response of microbial community composition and activity in agricultural and grassland soils after a simulated rainfall, Soil Biology and Biochemistry, 37, 2249–2262, https://doi.org/10.1016/j.soilbio.2005.02.038, 2005.
 - Szymanski, L. M.: Spatial Distribution and Long-Term Persistence of Ancient Carbon in Buried Soils and Its Vulnerability to Landscape Disturbance, Ph.D. thesis, University of Wisconsin-Madison, Madison, 2021.
 - Tsypin, M. and Macpherson, G.: The effect of precipitation events on inorganic carbon in soil and shallow groundwater, Konza Prairie LTER Site, NE Kansas, USA, Applied Geochemistry, 27, 2356–2369, https://doi.org/10.1016/j.apgeochem.2012.07.008, 2012.
- 650 Venables, W. N. and Ripley, B. D.: MASS (Modern Applied Statistics with S), https://CRAN.R-project.org/package=MASS, 2002.
 - Wahab, L. M., Kim, S., and Berhe, A. A.: Carbon and Nitrogen Dynamics in Subsoils After 20 years of Added Precipitation in a Mediterranean Grassland, https://doi.org/10.5194/egusphere-2024-3607, 2025.
 - Xiang, S.-R., Doyle, A., Holden, P. A., and Schimel, J. P.: Drying and rewetting effects on C and N mineralization and microbial activity in surface and subsurface California grassland soils, Soil Biology and Biochemistry, 40, 2281–2289, https://doi.org/10.1016/j.soilbio.2008.05.004, 2008.
 - Zhu, B. and Cheng, W.: Impacts of drying–wetting cycles on rhizosphere respiration and soil organic matter decomposition, Soil Biology and Biochemistry, 63, 89–96, https://doi.org/10.1016/j.soilbio.2013.03.027, 2013.